Earth Surface Dynamics
Open Access
Discussions

The hydrological cycle in the high Pamir Mountains: how temperature and seasonal precipitation distribution influence stream flow in the Gunt catchment, Tajikistan

E. Pohl[1], M. Knoche[2], R. Gloaguen[1,3], C. Andermann[4], and P. Krause[5]

[1]Remote Sensing Group, Geology Institute, Technische Universität Bergakademie Freiberg, B.-von-Cotta-Str. 2, 09599 Freiberg, Germany
[2]Helmholtz Centre for Environmental Research (UFZ), Halle, Germany
[3]Remote Sensing Group, Helmholtz Institute Freiberg of Resource Technology, Germany
[4]Helmholtz Centre Potsdam, German Research Centre for Geosciences (GFZ), Germany
[5]Gewässerkundlicher Landesdienst, Hochwassernachrichtenzentrale, Thüringer Landesamt für Umwelt und Geologie (TLUG), Germany

Discussion Paper | Discussion Paper | Discussion Paper | Discussion Paper

ESURFD
2, 1155–1215, 2014

Hydrological cycle of the Central Pamirs
E. Pohl et al.

Title Page

Abstract | Introduction
Conclusions | References
Tables | Figures

|◄ | ►|
◄ | ►

Back | Close

Full Screen / Esc

Printer-friendly Version
Interactive Discussion

Correspondence to: E. Pohl (eric.pohl@geo.tu-freiberg.de)

Discussion Paper | Discussion Paper | Discussion Paper | Discussion Paper | Discussion Paper |

ESURFD

2, 1155–1215, 2014

Hydrological cycle of the Central Pamirs

E. Pohl et al.

Title Page

Abstract	Introduction
Conclusions	References
Tables	Figures

|◄   ►|

◄   ►

| Back | Close |

Full Screen / Esc

Printer-friendly Version

Interactive Discussion

Abstract

Complex climatic interactions control hydrological processes in high mountains that in their turn regulate the erosive forces shaping the relief. To unravel the hydrological cycle of a glaciated watershed (Gunt River) considered representative of the Pamirs' hydrologic regime we developed a remote sensing-based approach. At the boundary between two distinct climatic zones dominated by Westerlies and Indian summer monsoon, the Pamir is poorly instrumented and only a few in situ meteorological and hydrological data are available. We adapted a suitable conceptual distributed hydrological model (J2000g). Interpolations of the few available in situ data are inadequate due to strong, relief induced, spatial heterogeneities. Instead we use raster data, preferably from remote sensing sources depending on availability and validation. We evaluate remote sensing-based precipitation and temperature products. MODIS MOD11 surface temperatures show good agreement with in situ data, perform better than other products and represent a good proxy for air temperatures. For precipitation we tested remote sensing products as well as the HAR10 climate model data and the interpolation-based APHRODITE dataset. All products show substantial differences both in intensity and seasonal distribution with in-situ data. Despite low resolutions, the datasets are able to sustain high model efficiencies (NSE ≥ 0.85). In contrast to neighbouring regions in the Himalayas or the Hindukush, discharge is dominantly the product of snow and glacier melt and thus temperature is the essential controlling factor. 80 % of annual precipitation is provided as snow in winter and spring contrasting peak discharges during summer. Hence, precipitation and discharge are negatively correlated and display complex hysteresis effects that allow to infer the effect of inter-annual climatic variability on river flow. We infer the existence of two subsurface reservoirs. The groundwater reservoir (providing 40 % of annual discharge) recharges in spring and summer and releases slowly during fall and winter. A not fully constrained shallow reservoir with very rapid retention times buffers melt waters during spring and summer. This study highlights the importance of a better understanding of the hydrologic cycle to constrain

natural hazards such as floods and landslides as well as water availability in the down-stream areas. The negative glacier mass balance ($-0.6\,\mathrm{m\,w.e.\,yr^{-1}}$) indicates glacier retreat, that will effect the currently 30 % contribution of glacier melt to stream flow.

1 Introduction

The Amu Darya, the main river draining the Pamir Mountains ("Pamirs") to the west, provides water resources for hydropower and irrigation along its way to the Aral Sea. The hydrological regime is reported as snow and glacier melt dominated (Lutz et al., 2014; Kure et al., 2013; Tahir et al., 2011), however, quantitatively largely uncon-strained. Increasing demand for water and assumed changes in hydrological regimes of glaciated catchments with respect to a change in climatic conditions (Immerzeel et al., 2009; Hagg et al., 2013) as well as the inherent increased risks demand for a better understanding of the processes governing surface flow in the region. More-over, the unique setting of the Pamirs in the transition zone between the Westerlies in the west (in the winter half-year) and the Indian summer monsoon (ISM) in the south (in the summer half-year) (Fuchs et al., 2013; Aizen et al., 2009; Syed et al., 2006; Palazzi et al., 2013; Mischke et al., 2010) make the Pamirs an outstanding natural laboratory to study aspects of the hydrologic cycle under different climatic influences.

There is a consensus in the characteristic change in the hydrologic regime along the Himalayan front from rainfall to snow and glacier melt dominated systems towards the west (Xiao et al., 2002; Bookhagen and Burbank, 2010; Lutz et al., 2014; Immerzeel et al., 2009). The few hydrologic studies in the Pamirs hence are basically glacier-/snowmelt-runoff models that relied on in situ data (Hagg et al., 2007) and, more recent, on GCM (Global Climate Model) data output (Kure et al., 2013; Hagg et al., 2013; Lutz et al., 2013) including future climate change scenarios. Different to the qualitatively agreeing hydrological studies, studies focusing solely on glaciers in the Pamirs show ambiguous results. Gardelle et al. (2013) e.g. state a slight mass gain for glaciers in the Pamir and also the Kharakorum region for the last decade. On the other hand

Lutz et al. (2013) and Sorg et al. (2012) report negative glacier mass balances for the Abramov Glacier in the north-eastern part of the Pamirs, however, for a slightly earlier time period.

Similar regional erosion rates along the Himalayan escarpment and the Pamirs (Herman et al., 2013) for the last 2Myr are surprising, considering the climatic and tectonic differences today. While order of magnitude higher precipitation amounts in the Himalayas do not allow a clear picture of how climate defines landscape evolution (Godard et al., 2014), the much drier climate in the Pamirs provides fundamentally different boundary conditions and suggests water availability as a limiting factor (Fuchs et al., 2014).

Precise knowledge of the spatiotemporal distribution of single components of the hydrological cycle would hence be of great benefit for any scientific field dealing with water transport and availability. This includes uncertainties about the role of climate in mountain evolution to differentiate between climate and more importantly climate variability and its potential strong impact on earth surface processes (Champagnac et al., 2012; DiBiase and Whipple, 2011; Montgomery and Brandon, 2002).

Due to the coarse resolution of the GCMs of several tens of kilometres, these datasets are usually downscaled before being applied in hydrological studies. This is especially demanded to catch melting processes along elevation gradients in heterogenous mountainous areas. GCM and remote sensing data provide the advantage of not needing numerous meteorological stations for interpolation because they provide data extensively. However, when downscaling is required, a proper transfer function is needed which is not trivial in mountainous regions. Wood et al. (2004) give a good example how diverse results can be resulting from different downscaling approaches in heterogenous areas, leading to a few hundred percent of over- or underestimation. The same is also true for interpolation of in situ data depending on what temperature lapse rates and precipitation gradients are applied (Immerzeel et al., 2014). Furthermore, the big differences in GCM and remote sensing datasets (Palazzi et al., 2013; Ménégoz et al., 2013) actually demand for a validation with in situ data, which sometimes

might not be available. Newly developed Regional Climate Models (RCM) such as the HAR10 (Maussion et al., 2014) help preventing inaccurate interpolation, but available time spans and spatial coverage are limited due to the high computational expense that is needed to create such datasets.

5   The abundance and increasing accuracy in GCMs, RCMs, and remote sensing data led to to their greater use in hydrological modelling (Khan et al., 2011; Awange et al., 2011; Liu et al., 2012; Bookhagen and Burbank, 2010) and glacier studies (Gardelle et al., 2012, 2013; Lutz et al., 2014; Sorg et al., 2012). In cold, arid, mountainous regions, GCMs are often favoured over remote sensing data. This is due to difficulties

10   in snowfall (Prigent, 2010), and snow water equivalent (SWE) retrieval (Takala et al., 2011; Tong et al., 2010) from space. Furthermore, direct measurement of ground air temperature from space is not possible. Remote sensing land surface temperatures (LST) are, however, being used to e.g. derive temperature lapse rates for interpolation of in situ data (Liu et al., 2012), or the calculation of evaporation (Samaniego et al.,

15   2011). Use of LST as a proxy for ground air temperature has also been established, however only in lowlands (Deus et al., 2013).

This paper concentrates on resolving the hydrologic cycle in the high mountains of the Pamir using a conceptual distributed hydrological model. This approach is very demanding due to data scarcity, and hence a special focus is set on the validation

20   of independent daily raster data from remote sensing, climate models, and combined products. The limited possibilities and problems (Tustison et al., 2001) to validate the specific raster datasets with in situ measurements are accounted for by an analysis of their influence on systematic effects in the resulting hydrological models. We ultimately aim for a conceptual description of the hydrological cycle in the Gunt and Shakhdara

25   river catchments (Fig. 1), considered as representative for the central Pamirs.

The advantages of using remote sensing and state-of-the-art RCM data with extensive spatial coverage stand against the limited time spans they cover. The earliest dataset used in this work starts in late 1997, but the required overall data superimposition was not achieved before the year 2000. A second reason is the relatively coarse

spatial resolution of such climatic datasets. For the Pamir region, raster data with resolutions ranging from 0.05° (≈ 4 km) to 0.75° (≈ 67 km) were available.

2   Study area

We select the Gunt catchment including its main tributary, the Shakhdara River located
5 in the central Pamirs (Fig. 1), because it is representative of the region in terms of
land cover and relief. The catchment is located in the south of the Gorno-Badakhshan
Autonomous Oblast (GBAO) in south-eastern Tajikistan (37° N/73° E), Pamir (Fig. 1). It
extends over about 14 000 km^2. The rivers Gunt and Shakhdara connect before they
flow through Khorog where an available gauging station is located. The catchment is
10 characterised by elevations ranging between 2080 m a.s.l. at the catchment outlet and
up to 6700 m a.s.l. at mount Karl Marx in the Shakhdara Range with an average of
about 4300 m a.s.l. The higher elevations are bounding the catchment but high elevations also occur within the catchment in the Shugnan Range that divides the Gunt
and Shakhdara sub-basins. Four meteorological stations are located in the watershed,
15 providing precipitation and temperature data for comparison and calibration of remote
sensing data. Three further stations are located in the vicinity of the watershed providing additional ground validation (Fig. A1).

The region is mainly influenced by two atmospheric circulation systems – Westerlies
alone in the western part and Westerlies in combination with the northward ISM in the
20 eastern part (Aizen et al., 2009; Palazzi et al., 2013; Syed et al., 2006; Fuchs et al.,
2013; Mischke et al., 2010). The ISM extension reaching the eastern part of the Pamirs
(Murghab and Shaimak) in summer provides less precipitation compared to the Westerlies in the western part (Khorog and Navabad) in winter (Fig. A1). Being at an average
altitude of 4300 m, the region is characterised by a long lasting snow cover. The in situ
25 data from 2000, and 2002 to 2006, provided by the State Administration for Hydrometeorology of Tajikistan (SAHT), show a distinct intra-annual distribution with a precipitation maximum in the winter half-year for the most-western stations Ishkashim, Khorog,

Navabad and Dzaushangoz. For the most-eastern stations Murghab and Shaimak a slight maximum in the summer half-year is noticeable. Based on oral information given by locals, highest precipitation might occur in the valleys rather than on the escarpments in the area around Khorog and Navabad. In general, there is a negative temperature gradient from west to east accompanying a positive trend in altitude. Station Bulunkul shows exceptionally low values of both precipitation and temperature, which is most likely induced by the orographic barrier surrounding lake Bulunkul. After Köppen-Geiger, Khorog, Navabad, and Ishkashim are characterised by a cold climate with hot and dry summers (Dsa), while Dzaushangoz and more eastern stations correspond to arid, cold, desert climate (BWk) (Peel et al., 2007). Due to the long lasting snow cover, as a result of Westerlies-induced winter precipitation and low temperatures (Immerzeel et al., 2009; Pu et al., 2007; Xiao et al., 2002), snowmelts are expected to play an essential role in the water balance. Even though the most eastern parts receive higher fractions of summer precipitation, high altitude and according temperatures below freezing temperature (Fig. A1) still suggest a substantial amount of precipitation received as snow.

3 Methods

We first present the hydrological model J2000g and its framework JAMS (Jena Adaptable Modelling System) followed by a description of the input data and their structures in a second part.

3.1 Hydrological modelling

Based on the area of interest, choices have to be made regarding the computational and distributional concept, as well as the model's temporal resolution. Daniel (2011) gives a good comparison of different frequently used models but the amount of different models is simply too big to be covered entirely.

The integration of raster datasets has been implemented in different models such as the MIKE SHE (Cooper et al., 2006; Liu et al., 2012) or CREST model (Khan et al., 2011), and several more examples of raster data input are available (Merritt et al., 2006; Stahl et al., 2008; Wood et al., 2004). While each of these models has specific quali-
5   ties, none of them is globally outperforming the others. The majority of existing models require very specific and scarcely available information on specific properties of for example soils and plants. We only have limited information available about these properties. Hence, we chose the conceptual distributed hydrological model J2000g within the JAMS framework because it is adapted to multi-scale hydrological studies and be-
10 cause soil and plant properties are simply and robustly integrated. More importantly, it allows the input of raster datasets (Krause et al., 2010) and to adapt some model components to the study area. Similar approaches have successfully been implemented in flat, semi-arid terrain (Deus et al., 2013) but also in heterogenous mountainous regions (Nepal et al., 2014).

15 ## 3.2   The JAMS framework and the hydrological model J2000g

The hydrological model J2000g (Kralisch et al., 2007; Krause and Hanisch, 2009) is modular-based and allows, to a certain degree, the interchange of specific modules to fit the user's needs. It uses a smaller number of calibration parameters than the fully-distributed J2000 model, which has been successfully applied in a similar complex
20 environment, the central Himalayas (Nepal et al., 2014). We chose J2000g over J2000 due to limited information on soil and aquifer properties. J2000g requires spatially distributed information about relief, land use, soil type, and hydrogeology to estimate specific attribute values for each entity or hydrological response unit (HRUs) (Krause and Hanisch, 2009). The required meteorological inputs are precipitation, minimum, maxi-
25 mum and average temperature, sunshine duration, wind speed, and relative humidity from one or more point sources. Usually, these data are then interpolated to provide data for each HRU. We avoid the interpolation thanks to area-wide coverage of raster data.

A conceptual outline of the modelling approach with superimposed meteorological data for the study area and their different spatial resolutions is given in Fig. 2. For each HRU a set of modules calculate the discharge components, evapotranspiration and storage changes. To improve model efficiency, parameters (Table 1) can be adjusted to account for inaccurately set values of soil, plant and hydrogeological properties. The substantial processing routine of J2000g consists of the calculation of net radiation based on Allen et al. (1998), followed by the calculation of potential evaporation (potET) after Penman–Monteith. Discrimination of precipitation as rain or snow is based on a threshold value T_{base} that is to be determined in the calibration process. Snow and ice melt are calculated using a day-degree method based on time-degree-factors (TMF) according to:

$$\text{melt} \, [\text{mm day}^{-1}] = \text{TMF} \times (T_{air} - T_{base}) \tag{1}$$

where T_{air} is the air temperature. A total of three TMFs are introduced in the model, one for snow of regular HRUs, i.e. non-glaciated HRUs, one for snow of glacier HRUs, and one for ice of glacier HRUs. The discrimination of two TMFs for snow accounts for wrongly assessed temperatures at high elevations resulting from averaged values of coarse resolution temperature data.

Meltwater and liquid precipitation are transferred to the soil water module, which consists of a simple water storage with a capacity derived from the field capacity of individual HRUs. Water stored in the soil, within the range of the storage capacity, can only leave through evapotranspiration. The calculated actual evapotranspiration (actET) depends on the saturation of the soil water storage, the potET, and a calibration parameter ETR. The soil storage must be saturated before runoff generation can start. The water amount exceeding the soil water storage is distributed into a lateral and a vertical component, based on the HRU's slope and the calibration factor LVD (Lateral-Vertical-Distribution). The vertical component is considered as percolation and is transferred to the groundwater storage component. The maximum amount of percolation is limited by the calibration parameter maxPerc. Base flow Q_{bas} is simulated with a linear outflow

routine adjusted by the recession parameter GWK (groundwater turnover time), which is defined as

$$\mathrm{GWK}\,[\mathrm{days}] = \frac{V}{Q},\qquad (2)$$

where V is the storage volume in mm, and Q is the outflow from this storage in mm day^{-1}. The lateral excess water is direct runoff Q_{dir}. J2000g's soil module expects well evolved soils with pronounced field capacities which are not the case in the Pamirs. Little vegetation on loose sediments, alluvial fans, and reworked moraine material result in a short retardation of water input and rather small field capacities (calibration factor FCA). We account for that by including a second linear storage component. The fast recession storage is calibrated with GWK1, and the second slow recession component with GWK2, respectively. J2000g treats both components as groundwater storages and hence we use the terms Q_{bas1}, and Q_{bas2} for the resulting discharge from these components. Percolation water enters the two linear storage component based on the distribution coefficient gwStorAlpha. In the end, Q_{dir} and the two Q_{bas}-components of each HRU are summed up to give the total simulated streamflow Q_{tot}.

J2000g does not have water routing through individual HRUs in a topological context like more complex models such as J2000, which however needs a more extensive parameterisation and according information. As a result, the J2000g model cannot account for losses and transformations during runoff concentration. We accept this limitation due to limited information available about soil and hydrogeological properties and assumed quick runoff on steep slopes without complex re-infiltration processes between HRUs.

4 Data

We use HRUs based on raster cells. All needed parameters were processed in the R-environment (R Core Team, 2014) and finalised using open-source GIS software

(GRASS-GIS and QGIS). We use a spatial resolution of 0.01° to balance the computational expense vs. the resolving power of some datasets. Linkage of the meteorological raster data to the single HRUs was achieved by overlay. The static parameters are considered constant over the time of the study and are provided once. All meteorological
5 data fed to the model has daily temporal resolution. The parameter and meteorological input data used in this work are described in the following two sections. An overview of these data as well as their spatial and temporal resolution are given in Table 2.

4.1 Geographical model parameters

4.1.1 Elevation, slope and aspect

10 Elevation is taken from a SRTM (Shuttle Radar Topography Mission) DEM (digital elevation model) (Jarvis et al., 2008) with 90 m resolution http://srtm.csi.cgiar.org. Slope and aspect are derived from this DEM with GIS-software.

4.1.2 Soil

Soil data are taken from the Harmonized World Soil Database (HWSD) (FAO et al.,
15 2009) and from the Atlas of the Republic of Tajikistan (Narzikulov and Stanjukovič, 1968). A combination of the HWSD database and the classification from the atlas that referred to soils by occurrence (e.g. alpine meadow or high mountain desert) was used to parametrise the soil map. HWSD provides grain size distributions for the first 30 cm for all and also for the depths from 30 to 100 cm for most leptosoils subtypes.
20 To derive the field capacities that represent a parameter of the J2000g model, empiric tables of the soil mapping manual Bodenkundliche Kartieranleitung (KA5) (Ad-hoc-Arbeitsgruppe Boden, 2005) were used. First, the bulk density given by the HWSD was used to derive the dry density (Ad-hoc-Arbeitsgruppe Boden, 2005, p. 126). Then the soil type was determined by using a soil type diagram (Ad-hoc-Arbeitsgruppe Boden,
25 2005, p. 142) in which the grain size distributions were inserted to derive the according

soil types. The field capacities were derived as function of soil type and dry density (Ad-hoc-Arbeitsgruppe Boden, 2005, p. 344). In combination with the information from the HWSD, the depth of the soils in cm and the total water capacity in mm were extracted. We assume vertical homogeneity of all soils for the parameterisation of soil water capacity.

4.1.3 Land use

For land use, we extract the IGBP (International Geosphere Biosphere Programme) classification scheme, included in the combined MODIS dataset MCD12Q1 (Strahler et al., 1999). We use the 2005 classification, marking the middle of the investigation period.

The Gunt and Shakhdara catchments are sparsely vegetated by xeromorphic dwarf-shrubs. Field observations in August 2011 have shown that vegetation diversity and vegetation cover are very low (< 5 %). Closed vegetation cover could only be observed at the spatially limited alpine meadows on the plateau in the eastern part of the catchment (≈ 3800 m a.s.l.). Therefore, vegetation changes are assumed to have only minor impact on the hydrology. The major classes of the 2005 IGBP classification for the studied catchment are 7.5 % permanent snow and ice, 24.0 % grassland, and 67.6 % barren or sparsely vegetated area. Associated plants to the IGPB classes are derived from Agakhanyantz and Lopatin (1978) and Breckle and Wucherer (2006). The according plant characteristics are then taken from the online database PlaPaDa (Plant Parameter Data) (Breuer and Frede, 2003). These characteristics comprise values for albedo, stomata resistances, leaf area indices, plant heights, and root depths. For the different seasonal and monthly characteristics the assumption was made that due to long lasting snow cover from autumn to spring (Immerzeel et al., 2009) little to no plant transpiration would take place during this time. To simulate this effect, the stomata resistances values were increased from November to March.

4.1.4 Hydrogeology

Hydrogeological information was taken from the Atlas of the Republic of Tajikistan (Narzikulov and Stanjukovič, 1968). The study area comprises five lithologies and two other classifications, one for ice/snow and one for lakes. The ice/snow extent differed from the land cover classification. Therefore we reclassified mismatching areas for snow/ice in the hydrogeological map according to nearest neighbour adjacent lithologies. At this stage we have no quantitative hydrogeological information and rely on some literature values (Batu, 1998) and assign maximum percolation rates between 10^{-7} mm day^{-1} for magmatic rocks and 10^{-6} mm day^{-1} for Quaternary sediments. During the optimisation process, J2000g will calibrate the correction factor maxPerc.

4.2 Meteorological data

4.2.1 Precipitation

Based on work of Palazzi et al. (2013) and Ménégoz et al. (2013), who both emphasise radical differences in precipitation datasets from various sources in the high mountains of Asia, we include a total of three precipitation datasets, one remote sensing product, one interpolated dataset, and one climate model dataset, to assess their influence on the representation of the hydrological cycle.

Evaluation of the datasets by comparison with in situ data is impeded by the point-wise character of rain/snow gauges on the one hand and area averaged values of the raster data on the other hand (Tustison et al., 2001). Precipitation events taking place nearby the rain gauge might contribute to the dataset but are not recorded for the in situ measurement. A rain event that moves might also introduce a temporal error, as it will be recorded only within a restricted time frame at the measuring station. Furthermore, meteorological stations are located in the valleys and hence cannot record advective precipitation at high altitude. Different spatial resolutions of the used datasets

complicate a representative analysis even more. Carried out correlation analyses with in situ data consequently show no significant correlation on a daily basis. If intensities are added up to monthly values (Fig. A2), correlation increases, especially for the higher resolution dataset. The differences in the datasets and few in situ data prevent an in-depth evaluation.

We will later on show that the most important aspect of any given precipitation dataset is the total amount provided in the snow accumulation period, building up the snow stock that serves as the basis for snow melt. This allows all datasets, as long as winter precipitation makes up a realistic amount, to represent the hydrological cycle in a very similar way. We account for potential intensity inaccuracies by applying different correction factors between 1 and 1.5 to our precipitation datasets.

The TRMM (Tropical Rainfall Measuring Mission) Multi-satellite Precipitation Analysis (TMPA) product TRMM3B42 V7 (Huffman, 1997; Huffman et al., 1997, 2007) was chosen as remote sensing product due to its frequent use along the Himalayan front (Bookhagen and Burbank, 2010; Roe, 2005; Kamal-Heikman et al., 2007). The 3B42 algorithm uses a two step approach to compute precipitation distribution: (1) TRMM's Visible and Infrared Scanner (VIRS), TRMM Microwave Imager (TMI) orbit data, and TMI/TRMM Combined Instrument (TCI) calibration parameters produce monthly infrared (IR) calibration parameters in the first step. (2) These calibration parameters are then used to adjust merged-IR precipitation data of several geostationary satellites to derive 3 hourly and daily (derived from the 3 hourly) accumulated precipitation data in $0.25° \times 0.25°$ spatial resolution with full longitudinal coverage. The data is validated with selected ground-truth information. The newest version (V7) includes additional sources of passive microwave satellite precipitation over the previous version (V6).

Bookhagen and Burbank (2010) assessed TRMM3B42 V6 data to model discharge in the northern Himalaya in the Indus catchment and found good agreement between precipitation intensity and discharge. Roe (2005) reports agreement of TRMM with precipitation gauge measurements in the Himalaya. In comparison to the Himalaya, the Tajik Pamirs only receive little precipitation. As Prigent (2010) points out, the de-

tection of light rain rates and quantification of falling snow is in focus for improvement of accuracy. Detection problems of falling snow related to already existent snow cover has also been pointed out by e.g. Yin (2004). This problem is of special interest for the study area because low precipitation is recorded at the two highest stations, and

5 due to the low temperatures most of the precipitation is expected to fall as snow. However, the microwave imagers do recognise snowfall, but quality relies on the discrimination between frozen precipitation and antecedent snow cover (Skofronick-Jackson and Weinman, 2004).Other authors report an underestimation of precipitation in cases of intense snowfall in the Himalayas (Kamal-Heikman et al., 2007).

10 TRMM3B42 V7 data shows data records in winter, when precipitation must fall as snow due to low temperatures. These data records show single precipitation events rather than a constant signal that could be expected if the signal was the result of the snow cover (that is persistent throughout the winter). We simply cannot assess the accuracy of TRMM3B42 V7 intensities at this point, but chose this product to have

15 a remotely sensed product for our approach. To assess its quality performance we independently applied an interpolated and a climate model dataset for validation.

The interpolated dataset is the APHRODITE (Asian Precipitation Highly Resolved Observational Data Integration Towards Evaluation of Water Resources) Monsoon Asia Version 11 APHRO_MA_V1101 (Yatagai et al., 2009, 2012). The Monsoon Asia re-

20 gion with a spatial coverage of 15° S to 55° N and 60 to 155° E and a temporal coverage from 1951 to 2007 with daily temporal resolution was used. The product is a weighted interpolation product of ground-based precipitation gauge data. The weighing is based on horizontal distance and an orographic correction model. Andermann et al. (2011) demonstrates that APHRODITE Monsoon Asia V1003R1 is the best per-

25 forming precipitation dataset available for the central Himalayas and the successor dataset APHRO_MA_V1101 has also been applied for Himalayan wide glacier melt studies (Lutz et al., 2014).

The third dataset is the High Asia Reanalysis (Maussion et al., 2014) dataset. The data is a result of a dynamical downscaling of global analysis data (Final Analysis

data from the Global Forecasting System (National Centers for Environmental Prediction NOAA, US Department of Commerce, 2000); dataset ds083.2) using the Weather Research and Forecasting (WRF-ARW) model (Skamarock and Klemp, 2008). Hence the quality of HAR depends on the global analysis data used as initialisation, and the model's capability to simulate the atmospheric processes.

Maussion et al. (2011) have shown good correlation of HAR with rain gauge data despite occasional overestimation on the Tibetan Plateau. Hence HAR is assumed to show a good representation of seasonal patterns, however with the limitation to calibrate precipitation quantities. From the different spatial resolutions available (30 and 10 km), we use the 10 km version (HAR10) for precipitation without making use of the discriminated rain/snow parts as we leave this to be subject of the model optimisation. Mölg et al. (2013) show that HAR10 shows good agreement with automatic weather stations on the Tibetan Plateau, and therefore has a high potential for glacier studies.

Comparison of each dataset with in situ data shows that differences in monthly added up values for TRMM3B42 V7 and APHRO_MA_V1101 are very small (Fig. 3a). HAR10 overestimates intensities especially in winter. The ratio of an individual dataset and in situ data (Fig. 3b) reveals that HAR10, despite overestimating, shows a constant ratio to in situ data of ≈ 4 suggesting a rather systematical error. APHRO_MA_V1101 and TRMM3B42 V7 show varying ratios but a lesser volume mismatch. If assuming positive precipitation lapse rates a grid value of either dataset should overestimate observational data, because meteorological stations are located on the valley floors. However, HAR10 precipitation in its original version provided too much precipitation to the model, being unable to deal with resulting extremely high snowmelt amounts. Based on that we correct HAR10 precipitation intensities downward to obtain a ratio with in situ data of 1. This downward correction at the beginning is only conducted for HAR10 because the other datasets were able to simulate the hydrograph. In a second step we apply correction factors to all precipitation datasets to account for possible positive precipitation lapse rates. We apply factors ranging from 1 to 1.5 (see Table 3) and hereafter refer to the individual precipitation datasets according to their annual

average precipitation amount, e.g. HAR10 (172 mm) for the downscaled version with 172 mm average annual precipitation.

4.2.2 Temperature

We use two different datasets for air temperature, one derived from remote sensing data and one from a climate model dataset. The datasets are calibrated based on available in situ data. Remote sensing determination of air temperature at ground level is not available at a global scale. Land surface temperatures (LST) on the other hand can be determined from surface emitted thermal infrared radiation that can pass through the atmosphere, and can thus be measured with appropriate instruments from space. We therefore correlate LST with in situ data to use them as a proxy for air temperatures.

The LST dataset is the MODIS MOD11C1 V5 (Wan and Li, 1997; Wan et al., 2004; Wan, 2008) data that provide night and daytime LST along with emissivity. The data is available as $0.05°× 0.05°$ resolution Climate Modelling Grid (CMG) in daily temporal resolution. The determination of the LST is based on the thermal infrared (TIR) radiation emitted by the surface in combination with the emissivity of the surface material. Information from other MODIS products e.g. land cover (MOD12), snow cover (MOD10) and cloud mask (MOD35) is incorporated in the algorithms (Wan, 2008). We chose the MOD11C1 V5 over the MOD11C1 V4 dataset due to better spatial coverage and improvements for high altitude (Wan, 2008). Missing values that occur mainly due to cloud cover or missing files in the dataset were temporally interpolated using smoothing splines from R's stats-package (R Core Team, 2014). The method was applied to each grid cell/pixel. Applicability of using LST as a proxy for air temperature has been demonstrated for example by Kawashima et al. (2000); Mostovoy et al. (2006); Deus et al. (2013).

The climate model dataset is the HAR10 2 m air temperature data. It is based on the same downscaling method used for HAR10 precipitation that was mentioned before. Due to HAR10's reported usefulness for glacier balance studies (Mölg et al., 2013) and good representation of snow cover on the Tibetan Plateau (Maussion et al., 2011),

along with a distinct correlation with in situ data (Fig. 4), we include this dataset to see if it provides a good all-in-one solution for the two key meteorological drivers. Correlation with in situ temperatures is expectedly lower than compared to MODIS MOD11C1 V5 because of HAR10's coarser spatial resolution of 10 km, and hence averaged values over a larger spatial domain.

Our comparison of LST with in situ air temperature shows high correlation ($R^2 = 0.83$ for all pixels encompassing meteorological stations) (Fig. 4). Pronounced underestimation for lower temperatures reduces the overall slope. This leads to an increased underestimation for higher temperatures. Therefore, we apply a linear regression with a fixed slope of one (linear model 1) to have a more representative dependency for the more important higher temperatures (affecting freezing, melting, and evapotranspiration). Based on the regression analysis we calibrate the LST dataset to match the observed air temperatures from the meteorological stations. Comparison of HAR10 and in situ data show a similar characteristic and hence we apply the same correction procedure.

4.2.3 Windspeed and relative humidity

Windspeed and relative humidity data are based on the NOAH Land Surface Model (Chen and Dudhia, 2001; Chen et al., 2007; Ek et al., 2003) from Global Land Data Assimilation System (GLDAS) (Rodell et al., 2004). We use the GLDAS_NOAH025SUBP_3H (Hydrological Sciences Branch at NASA/Goddard Space Flight Center , GSFC/HSB) dataset provided in 3 hourly temporal and 0.25° × 0.25° spatial resolution. The data basis are various satellite and in situ data (for more information see: http://mirador.gsfc.nasa.gov/collections/GLDAS_NOAH025SUBP_3H__001.shtml).

The extracted 3 hourly windspeed data were simply averaged to daily data. For relative humidity, further calculations had to be performed as GLDAS_NOAH025SUBP_3H only provides specific humidity. Water vapor and atmospheric pressures are needed to calculate relative humidity from specific humidity (Häckel, 1999). However,

GLDAS_NOAH025SUBP_3H does not provide vapour pressure. Relative humidity was therefore calculated based on information provided by the LP DAAC (Land Processes Distributed Active Archive Center) (see Appendix A).

4.2.4 Sunshine duration

For sunshine duration, coarse (0.75° × 0.75°) ECMWF (European Centre for Medium-Range Weather Forecast) ERA Interim data were obtained from ECMWF servers. ERA Interim data incorporate modelled climate data from a wide range of satellite and in situ measurements (Dee et al., 2011). Sunshine duration is demanded by the model intern calculation of global radiation by acting as a proxy for cloudiness to reduce the internally calculated extraterrestrial radiation.

5 Model calibration

The JAMS framework utilises the Shuffled Complex Evolution method of the University of Arizona (SCE-UA) (Duan et al., 1994), which is systematically approaching a best calibration for model optimisation (Fischer et al., 2009). A set of given values for the calibration parameters will result in a certain realisation of a chosen efficiency criterion. All possible realisations will span a surface in a $n + 1$ dimensional space, where n is the number of calibration parameters. The SCE-UA algorithm searches for the optimal calibration that is given by the global maximum or minimum (depending on wether the efficiency criterion has to be maximised or minimised) of this surface. The name shuffled complex derives from multiple sets of points (complexes) that are used to approach the extrema. The points that belong to a complex are shuffled every iteration (evolution) enabling the algorithm to search the surface in a very efficient way as has been shown by Duan et al. (1994). The Nash–Sutcliffe efficiency (NSE) (Nash and Sutcliffe, 1970) was chosen as efficiency criterion.

The observed discharge for the NSE calculation is based on daily discharge measurements conducted on a daily basis with few exceptions since 1960 in Khorog (Fig. 1). We cannot independently assess the quality of the measurements, but old equipment along with old rating curves imply a possible source of error. Anthropogenic influences on the observed discharge are most probably minor but hard to assess. A hydro-power plant and a lake regulation station are operating near site Navabad and close to Bulunkul at lake Yashilkul. While the amount of water used by the power plant would return to the river without change in quantity and without noticeable recession, no particular information on the lake regulations are available but few available records from the 1960s show similar winter discharge as in the 2000s. Other anthropogenic influences are irrigation, which is occurring during summer and almost exclusively in the valleys, but is assumed to be of minimum impact due to the low population density.

The same SCE optimisation procedure is conducted for all model setups. We always add an additional amount of 300 mm to a used precipitation dataset at the beginning of the modelling period to account for empty groundwater storages and snow stocks. For the earlier starting setups with temperature from MOD11C1 V5 this is on 1 March 2000 and for the setups with HAR10 temperature on 1 January 2001. The spin-up phase is either two years for the former or one year for the latter setups. Similar baseflow and snow stock values for the models with different temperature data suggest sufficient spin-off time for the setups with HAR10. The actual calibration is then restricted to the period from 2002 to 2007.

6 Results

The majority of the optimised models were consistent in their representation of the hydrological cycle and required similar calibration parameters. All models agreed on a substantial amount of groundwater discharge and a characteristic transition from snow to glacier melt during summer. Strongest differences can be observed if significantly different amounts of winter precipitation are provided. The fact that cold temper-

atures during winter prevented any liquid precipitation and snow or glacier melt, implied a strong constraint on the parameterisation of the groundwater aquifer. Low winter precipitation resulted in increased glacier melt and vice versa. Modelled variabilities in the well pronounced intra-annual cycle were consistent between different models and in-

5 dependent of the used precipitation dataset. This highlights the temporal decoupling of precipitation and discharge, and a strong influence of temperature on the modelling.

6.1 Modelling results

Best NSE and lowest RMSE were obtained using a combination of MOD11C1 V5 temperature and HAR10 (258 mm) precipitation (Table 1). Setups with MOD11C1 V5 tem-

10 perature consistently resulted in better NSE and 7 to 15 % smaller RMSE (Root Mean Squared Error) than setups with HAR10 temperature. The hydrological cycle according to the best obtained model results is shown in Fig. 7. Starting at the end of autumn, all precipitation is being accumulated as snow cover. During this time Q_{tot} results entirely from Q_{bas}. In late spring the melting season starts with high peak discharges and

15 replenishment of the groundwater reservoir. During the middle of the melting season snowmelt transitions into glacier melt. Finally, at the end of summer, there is no snow cover left and melt water only originates from glacier melt before the cycle starts again. Because glacier melt directly became Q_{dir} in the model, it could not infiltrate into soils and storage components. As a result only snowmelt and rainfall contributed to ground-

20 water replenishment.

Smallest deviations for cumulative discharge were observed for models with precipitation from HAR10 (258 mm). For setups with TRMM (308 mm), a higher underestimation in 2002 and 2004 compared to HAR10 (258 mm) and APHRO (200 mm) was observed where SWE values were also much smaller. Use of APHRO (200 mm) resulted

25 in the highest underestimation, which is most pronounced in winter. Higher glacier melt in summer for setups with APHRODITE_MA_1101 precipitation reduced this underestimation in summer. The higher fraction of summer precipitation for TRMM3B42 V7 and APHRODITE_MA_V1101 was accompanied by a higher contribution of glacier runoff

to total discharge and more negative glacier mass balances (Fig. 5). All models showed highest deviations from observed discharge in 2006 and 2007, which might be related to the mentioned lake level regulations. However, no validation data was available.

Comparison of the best individual model setups regarding their inputs and outputs are presented in Fig. 5. Best models showed a higher fraction of snowfall over rainfall. A particular precipitation dataset showed higher snowfall proportions ($\approx 10\%$) with MOD11C1 V5 temperatures compared to HAR10 temperatures. Despite the big differences in snow fraction, values for Q_{bas1} (resulting from snow melt) showed comparable results of ≈ 20 to 30% of Q_{tot}. An exception was the model using the combination of HAR10 temperature and HAR10 (258 mm) precipitation with 42% Q_{bas1}. This was accompanied with the longest recession coefficient for the fast recession subsurface flow (GWK1) of ≈ 38 d compared to values between 14 and 30 d for models with HAR10 temperature and values between 10 and 19 d with MODIS temperatures (Table 4). Despite this deviation and despite the difference between the proportions of Q_{bas1} to Q_{bas2} for either temperature datasets, all models showed high consistency for (1) the sum of Q_{bas1} and Q_{bas2}, (2) the ratio of Q_{bas} over Q_{dir}, (3) the proportion of Q_{glac} to Q_{tot}, and (4) the glacier mass balances. Only actET and the volume errors showed noticeable differences.

The groundwater proportion in the hydrological cycle (Q_{bas2}) made up $\approx 40\%$ of Q_{tot} with the exceptions of the model setups using only HAR10 data and the models using APHRO (200 mm) (Fig. 5). Glacier mass balances show a factor 2 difference. Smallest losses of -0.6 m w.e. yr^{-1} were obtained with HAR10 (258 mm). Highest losses of -1.2 m w.e. yr^{-1} were obtained with APHRO (200 mm) that also showed the strongest negative volume errors of $\approx -9\%$. Since this indicates a strong underestimation of the already upward corrected APHRO (200 mm) dataset, we do not think that obtained model results of APHRO (200 mm) are representative of the hydrological cycle.

Title Page

Abstract | Introduction

Conclusions | References

Tables | Figures

|◄ | ►|

◄ | ►

Back | Close

Full Screen / Esc

Printer-friendly Version

Interactive Discussion

6.2 Dataset characteristics

The precipitation datasets show different spatial and seasonal distributions. TRMM3B42 V7 and APHRO_V1101_MA both show a similar seasonal distribution (Fig. 5) while HAR10 has ≈ 20 % more precipitation in winter and spring combined and only 8 % of its annual precipitation is provided in summer, compared to 23 % for TRMM3B42 V7 and APHRO_V1101_MA.

The average annual discharge volume is 3.48 km^3 yr^{-1} (= 255 mm yr^{-1}). Only TRMM (308 mm) (= 4.2 km^3) and the original HAR10 dataset (688 mm) (= 9.38 km^3) provide more precipitation. Small precipitation amounts provided by APHRO (152 mm) and APHRO (200 mm), together with a high fraction of summer precipitation resulted in little water being accumulated in snow stocks for these model setups. In the SCE-UA optimisation these small snow stocks were then compensated by increased glacier runoff with the earliest start (late spring) amongst all model setups. Even though the initially downwards corrected HAR10 (172 mm) data provided only little more precipitation than APHRO (152 mm), its more pronounced winter distribution led to higher snow stocks and less pronounced glacier melt. All presented HAR10 datasets (except for the original one with 688 mm precipitation), as well as both APHRODITE datasets outperformed the original TRMM (308 mm) data (Table 4).

MODIS MOD11C1 V5 night LST showed higher correlation with in situ data than HAR10 temperature (Fig. 4), and all model setups with a particular precipitation dataset showed higher NSE if used together with MOD11C1 V5 instead of HAR10 temperatures (Fig. 5, Table 4).

6.3 Sensitivity analysis

Our sensitivity analysis is based on the convergence or non-convergence of calibration parameters and their value range obtained with the SCE-UA method with NSE as optimisation criterion. Three groups of parameters can generally be differentiated. These groups are the ones determining (1) snowmelt, (2) glacier melt, and (3) groundwater

properties. At the beginning of the hydrological cycle, the snow melt parameters dominate the representation of the hydrogrpah. That is because snow melt is the main contributor to river discharge. Then, depending on how much snow is available for melting processes, glacier melt has to start earlier or later to counter over- or underestimation. Last, depending on when, and how much water is available by means of snowmelt, respective groundwater parameters have to ensure to retard and adjust the water release correctly. The parameterisation is thus most dependent on the used precipitation dataset.

We used a set of 12 calibration parameters (Table 1) and 8 complexes that showed converging parameter values after 4000 to 5000 runs and showed not more than 1 % improvement in NSE later on. With little idea about specific soil and aquifer properties, all related soil and groundwater parameters were included in the SCE-UA optimisation process. Wide value ranges for the calibration parameters allowed for possible equifinality. Figure 6 shows the parameter calibration for both temperature datasets independently. The best parameterisation as well as the value ranges for the individual best performing precipitation datasets are highlighted. When considering all of the applied temperature and precipitation datasets, the most restricted parameters were TMF_{gi} and LVD, followed by Tbase, FCA and $Tbase_g$. The most unrestricted parameters were the groundwater and the fast linear storage component related parameters GWK2, gwStorAlpha, maxPerc, and GWK1. Constraints for a certain parameter were largely independent of the used temperature dataset.

The degree-day-factor for glacier melt TMF_{gi} always showed a narrow value range of about $1\,mm\,°C^{-1}\,day^{-1}$. Degree-day-factors for snow were less constrained. The most obvious difference regarding the use of a specific temperature dataset were observed for the obtained threshold temperatures Tbase. Tbase for models with MOD11C1 V5 was about 2 to 3 °C higher than for models with HAR10 temperature. The threshold temperature for glaciers $Tbase_g$ did not show such a distinction between the different temperature datasets. Low precipitation volume datasets, such as APHRO (154 and 200 mm) and HAR10 (172 mm) led to lowest $Tbase_g$ values in the setups with

MOD11C1 V5. No such effect was observed with HAR10 temperature. The field capacity correction factor FCA, and the discrimination factor LVD for lateral or vertical distribution of soil excess water were both very low, i.e. the soil was modelled to store very little water and distribute the majority of this water to the underlying storage components. For the setups with MOD11C1 V5 the resulting values were (1) lower than for setups with HAR10 temperature, and (2) more constrained.

7 Discussion

Independent of the used datasets, i.e. whether interpolated, remote sensing, or regional climate model data was used, the models yield comparable and confident results regarding the representation of the hydrological cycle. There is, however, an important dependency of model performance with the amount of precipitation provided during the snow accumulation period in winter. Too high winter precipitations lead to the model failing to produce meaningful results. Low winter precipitations cause overestimated high glacier melts. The lack of in situ measurements does not allow us to determine the thresholds with certitude.

Most striking is the fact that the relationship of precipitation to discharge is expectedly variable for individual precipitation datasets (Fig. 8d), but the relationship of resulting liquid water input (from snow and glacier melt, and liquid precipitation) to discharge shows a high consistency (Fig. 8e). This consistency results from the dominant role of temperature as trigger for melt water and the overall delay between precipitation. To account for spring and summer discharge, melt is required that lead to slightly different model parameterisations to adapt to precipitation input. As the bulk of precipitation is provided as snow, but only released as melt water in summer, groundwater discharge is essentially the only contributor to river streamflow for the winter half-year.

7.1 Hydrological cycle

The different intra-annual distributions and amounts of precipitation of the individual datasets cause an ambiguous picture of the water input–output relationship. On the other hand, analysis of the individual water cycle components all agree on a substantial

5　amount of deep groundwater discharge (Q_{bas2}), a not yet fully constrained fast retention storage discharge (Q_{bas1}), and glacier runoff (Q_{glac}) (Fig. 5). This observation is best explained by comparing the temporal relationships of discharge with (1) precipitation, (2) with effective precipitation (P_{eff}) – defined as all liquid stream water contribution from rainfall, snowmelt, and glacier melt –, and (3) with temperature (Fig. 8a–f)

10　The concept of the hysteresis plots is that an immediate response of river discharge to water contribution into the system will result in plotted values along a 1 : 1-line. In contrast, if the different storage compartments induce a lag of response, the points are deflected from this 1 : 1-line and describe an hysteresis effect. Below the 1 : 1-line (less discharge than contribution) this describes a storage recharge, and above the 1 : 1-line

15　this describes a depletion of storage.

The overall best performing models with either TRMM3B42 V7 or HAR10 precipitation data, show a strong decoupling of precipitation and discharge (Fig. 8a, d) that results in an almost 90° rotated picture compared to the 1 : 1-relationship. This results in a water surplus from October to May and higher discharge than water input from

20　June to September. TRMM (308 mm) and HAR10 (258 mm) show a similar behaviour (Fig. 8d) with the biggest difference being a shift towards more precipitation for TRMM (308 mm). APHRO (200 mm) shows a systematically different behaviour that cannot be explained by a simple shift in precipitation amounts.

In comparison to precipitation, the relation between discharge and P_{eff} is more im-

25　mediate (Fig. 8b, e) and shows a similar shape to a rainfall-dominated system in the Himalayas (Fig. 8c). The anti-clockwise hysteresis for the rainfall-dominated catchment (Fig. 8c) depicts water retardation in aquifers as has been reported by Andermann et al. (2012b). The biggest difference between the Pamirs and the Himalayas is the

long flat tail of the hysteresis loop in winter (Fig. 8e) when stream flow almost entirely originates from groundwater discharge, while no effective precipitation occurs. The differences between the individual hysteresis loops with P_{eff} (Fig. 8e) for different precipitation datasets are smaller than for the hysteresis loops with actual precipitation (Fig. 8d). Using APHRO (154 mm) and HAR10 (172 mm) precipitation data results in systematically different shapes (shaded area at lowest specific discharge in Fig. 8e) which indicates a minimum threshold value for precipitation needed to obtain the systematic hysteresis loop with the long flat tail in winter. This underlines, above all, the elusiveness of quality assessment for precipitation datasets within glacier-/snowmelt-runoff studies if no cross-validations e.g. with snow cover data are conducted. It also leads to the conclusion that an accurate estimation of temperatures can vastly improve certainty in such studies. HAR10 and MODIS temperatures used in this study seem to provide good estimates but a validation with in situ data at very high altitude should certainly be in focus for future studies. The overall better performance of MODIS temperatures suggest that the finer resolution significantly improves the representation of the hydrological cycle, probably because snowmelts are captured better. However, the coarser resolution of HAR10 still proves itself to be a viable option. This might be of special interest for studies conducted for a larger extent. The strong dependence of discharge on temperature is shown in Fig. 8f. The dependency is not straightforward but shows a small clockwise loop in the summer half-year ($T > 0\,^{\circ}$C) and a small anti-clockwise loop in the winter-half year ($T < 0\,^{\circ}$C) along with different slopes for the individual half-years. Due to a decreasing snow stock in summer the meltwater response to a same temperature decreases. Given a same temperature in winter the initial higher groundwater storage will cause more discharge at the beginning of the season than towards the end.

Because our model prevents glacier runoff to infiltrate into the soil and subsequent storages, the winter groundwater discharge mainly originates from snowmelt of the preceding melting period. Changes in precipitation patterns and/or intensities towards less winter precipitation would therefore severely effect winter discharge of the consec-

utive year. Additionally, an increase in summer precipitation would not necessarily be noticed hydrograph-wise due to higher interception and evapotranspiration. This is also the reason why TRMM (308 mm) with a higher portion of summer precipitation in comparison to HAR10 (258 mm) produces more glacier runoff, and a more negative glacier

5 mass balance (and higher actET values) despite providing overall more precipitation.

Our results support findings of several studies that have pointed out a shift from rainfall towards more snow and glacier melt-dominated systems towards the west of the Himalayan syntaxis (Bookhagen and Burbank, 2010; Immerzeel et al., 2009; Lutz et al., 2014).

10 We also find similarities to findings by Andermann et al. (2012b), who state a big impact of groundwater discharge on the annual hydrological cycle in the Central Himalayans. Our modelled groundwater storage capacities (≈ 100 mm) are comparable to their findings for a high alpine glaciated but rainfall-dominated catchment. Groundwater turnover times of 200 to 400 days (GWK2) in this study correspond to typical

15 values found for fissured rock aquifers (Schwarze et al., 1999), which also characterise the Central Himalayan catchments (Andermann et al., 2012b).

We find substantial accordance with several glaciological studies in the Pamirs and its proximity. Haritashya et al. (2009) state average retreat rates of 10.9 m yr^{-1} (1976–2003) based on model predictions and imagery analysis for the Wakhan Range, just

20 south of the study area (Fig. 1), and Khromova et al. (2006) report a decrease in glacier area of 11.6 % (1990–2001) for the northern Pamir and a general negative mass balance trend for the Pamirs between 1970 and 2000. Lutz et al. (2013) used a regionalised glacier mass balance model to evaluate climate change scenarios in the Amu Darya catchment (comprising most of the Pamirs). They predicted ≈ -0.6 to

25 -0.7 m w.e. yr^{-1} for the period 2007 to 2017. Contradicting findings of Gardelle et al. (2013), stating positive glacier mass balances for the Pamir region between 1999 and 2011, might simply be related to the different study location further northwest around the Abramov and Fedchenko glaciers. This region is assumed to receive severely more precipitation compared to the region encompassing the Gunt and Shakhdara catch-

ments (Ménégoz et al., 2013; Fuchs et al., 2013) and hence provides a very different climatic setting. Sorg et al. (2012) on the other hand presented negative glacier mass balances for the Abramov Glacier of $\approx -1\,\mathrm{m\,w.e.\,yr}^{-1}$ for the period from 1970 to 1999. The quantification of the actual glacier mass balance should be addressed in the future to further validate the model.

We also find our modelled values for actET being corroborated by the work of Bookhagen and Burbank (2010), stating actET values less than $100\,\mathrm{mm\,yr}^{-1}$ for the Pamir region based on satellite derived data from MODIS. The precompiled MODIS MOD16 (Mu et al., 2011) product for evapotranspiration is not feasible in the study area because only values for vegetated areas are given (according to MODIS MCD12Q1 land cover classification $\approx 20\,\%$ of the study area).

7.2 Dataset characteristics

In contrast to TRMM and APHRODITE that show similar seasonal distributions, HAR10 provides 20 % more of its annual precipitation in the winter-half year (Fig. 5). This results in up to 86 % of precipitation provided as snow (modelled). Better performing models show higher fractions of precipitation as snowfall, which matches the assumption that most moisture is supplied by the Westerlies in winter and early spring (Immerzeel et al., 2009; Pu et al., 2007; Xiao et al., 2002). In its original version, HAR10 provides 450 % more average annual precipitation than APHRO_MA_V1101, and 220 % more than TRMM3B42 V7. Despite HAR10's overestimation, it is the only dataset that shows a strong correlation with in situ data on a monthly basis (Fig. A2). But it is also the only dataset that does not yield NSE > 0.8 in its original version (independent of the used temperature dataset). Very little snowmelt, on the other hand, as it is the case for setups with APHRO_MA_V1101 precipitation, was compensated by high glacier melt during most of the year. Both overestimation and underestimation of precipitations lead to improbable processes and lower model accuracies.

We cannot unrestrictedly favour TRMM3B42 V7 in return. Low snow stocks with TRMM3B42 V7 e.g. in 2002 and 2004 might be the result of TRMM's reported is-

sue on snowfall determination (Yin, 2004; Kamal-Heikman et al., 2007; Skofronick-Jackson and Weinman, 2004; Prigent, 2010). The fact that TRMM detects precipitation when there must be at least partial snow cover and hence the determination of falling snow should be problematic leads us to wonder what TRMM really records and with what confidence. We see a crucial need to validate/calibrate HAR10 and APHRO_MA_V1101 data against in situ measurements to not expect a high bias in the proximity to our study region. The use of these regional/global datasets for studies on glacier retreat and precipitation amounts in the entire Himalayan domain or the Tibetan Plateau (Mölg et al., 2013; Lutz et al., 2014) consequently raises issues about the representativeness of obtained results where there is no validation data available.

After correction, all used precipitation datasets yield high NSE (Table 4), underlining once more that the amount of precipitation provided by a dataset within the snow accumulation period is more important than the exact timing. In fact, a randomly resampled HAR10 (258 mm) dataset e.g. still yields an NSE of 0.76. The use of a different precipitation dataset still has a relatively high influence on the proportion of a particular water component compared to the negligible effect of a different temperature dataset.

7.3 Sensitivity and modelling concept

The model calibration with the SCE-UA method suggests a reliable parameterisation. Two striking observations were made. Firstly, very narrowly constrained values of $\approx 1\,\mathrm{mm}\,°\mathrm{C}^{-1}\,\mathrm{day}^{-1}$ for $\mathrm{TMF_{gi}}$ seem to contradict common literature values of 7 to $10\,\mathrm{mm}\,°\mathrm{C}^{-1}\,\mathrm{day}^{-1}$ (Hock, 2003). However, the simple glacier module does not account for the transformation of snow into ice. Most importantly, the resolution of 0.05° (MOD11C1 V5) and $\approx 0.09°$ (HAR10) of the temperature data causes the entire glacier surface to melt rather than the glacier termini. Secondly, very low values for FCA, and LVD withdraw the soil's water storage capacity and cause most of the water being transferred to the underlying linear storages. This results in almost no Q_{surf} (Fig. 5) and instead representation of retardation effects from refreezing of melt water in snow-

packs, frozen soils, and routing through sediment deposits by Q_{bas1}. Because the soil module used in J2000g is designed for well developed soils, it appears to be not useful in the presented environment.

Generally, the calibration accounts for the amount of precipitation provided by the different precipitation datasets by increasing or decreasing Tbase and especially Tbase$_g$ to make glacier melt start more early and thus accounting for too little snow stocks (for datasets with little precipitation). Even though individual model setups show minor differences in the contribution of single water components to total discharge, the resulting hydrographs are similar.

Overall, we find that the J2000g model is a good choice for our approach due to its simplicity and low number of calibration parameters compared to more physically-based models. The choice of a rather simple model is furthermore justified by the high level of uncertainties within the used precipitation datasets. From a technical point of view, the integration of various datasets in different spatial resolutions synergises with the chosen raster-based HRU approach. Due to the model's independency of the input raster's spatial resolution, datasets can easily be exchanged.

Regarding the model concept, we discover the need to introduce a low recession storage component as intermediate component between the deep groundwater and the soil. Even though not yet fully constrained, we introduce it to account for recession of subsurface flow in the numerous moraines and debris covered hillslopes, but also for refreezing of surface water mainly during night within the snow layer or frozen/permafrost soils. Little is known about erosion processes in Pamir. Knowledge about single water components and especially their variability is not just useful for further development of risk assessment (e.g. Gruber and Mergili, 2013) but also a potent instrument to study several aspects of mountain evolution. Because long term climate records might be insufficient to get a good idea about weather variability, this approach can provide a valuable tool to study short-term effects of weather on erosion. Now it is possible to relate mass transport in rivers to single water components with water provenance. Additionally, it could explain the outstanding discrepancy of intensities between hills-

Hydrological cycle of the Central Pamirs

E. Pohl et al.

Title Page

Abstract | Introduction

Conclusions | References

Tables | Figures

◀ | ▶

◀ | ▶

Back | Close

Full Screen / Esc

Printer-friendly Version

Interactive Discussion

lope erosion and river incision in the Pamirs (Fuchs et al., 2013, 2014). The primary control of tectonic-driven topographic steepness on erosion suggests that changes in water availability are balanced by complex interactions between channel steepness and width, and concentrated sediment transport (Burbank et al., 2003; Scherler et al., 2014). Additionally, in Pamir, while incision is sustained by a steady flow of groundwater discharge, buffering snow and glacier melts, hillslope material can only be mobilised during a few months when the temperatures generate melts that will be essentially transferred as runoff. Andermann et al. (2012a) demonstrated the role of intense precipitations on generating direct runoff and sediment supply from hillslopes in the Himalayas. In contrast, water availability in the Pamirs is spatiotemporally differentiated due to successive melting. This implies the need for spatiotemporal data to apply adequate modelling of erosion from snowmelt (Ollesch et al., 2005, 2006), and hillslope mass movements, such as landslides, which are related to soil moisture content (Iverson, 2000; Dietrich et al., 1992). Such coupled approaches might help to understand deep incision rates in the Pamir that are accompanied with rather preserved landscapes.

8 Conclusions

A combination of nested GCM and remote sensing data allows an accurate retrieval of the hydrological cycle using the J2000g model. With $\approx 80\%$ of precipitation being supplied as snow, the water input is dominated by snowmelt. The interaction of temperature and the spatiotemporal distribution of precipitation are the factors characterising the region's hydrology. The presented precipitation-discharge hysteresis emphasises this finding. The study area is dominated by Westerlies with a noticeable but minor ISM influence. The lag appearing during summer for the precipitation-discharge hysteresis reveals the influence of ISM on the system. Temperature is the principal trigger of discharge, originating from snow and ice melt.

Title Page

Abstract | Introduction

Conclusions | References

Tables | Figures

⏮ | ⏭

◀ | ▶

Back | Close

Full Screen / Esc

Printer-friendly Version

Interactive Discussion

Our analysis of different widely used precipitation datasets provides a valuable basis for further studies in western Tibet and similar environments. Key findings are (1) that APHRO_MA_V1101 underestimates actual precipitation by a factor ≈ 2 and should not be applied in the Central Pamirs, and (2) that HAR10 overestimates (factor 2 to 3) but shows a good representation of spatial distributions, and (3) that TRMM3B42 V7 suffers most likely from inaccurate precipitation retrieval over existing snow covers and is therefore not a good choice for the present environment. In summary, we find HAR10 to be the best choice for precipitation, but with the crucial need to downscale intensities. For temperature, both MODIS data as proxy for air temperature, and to a lesser extent because of its coarser resolution HAR10 temperature data provide reliable estimates of air temperature for snow and glacier melt studies that might be superior to simple spatial interpolation based on lapse rates.

$\approx 200\,mm$ (4/5) the annual discharge takes place in summer as a result of snow and glacier melt, and $\approx 50\,mm$ (1/5) in winter. Because winter discharge is mainly sustained by groundwater discharge, and because groundwater originates from snowmelt in summer, streamflow at any time of the year is originating from melting of snow and ice. This complicates the assessment of future water availability with respect to a shift from a melt- towards a more precipitation-dominated hydrological regime under climate warming. Common practice in water availability and risk studies is the application of long-term projections of temperature increase and their effect on melting processes (Gruber and Mergili, 2013; Kure et al., 2013; Immerzeel et al., 2013). Such projections do, however, not account for short-term weather variability, which we think might have a stronger impact on the occurrence of avalanches, floods, and water mobilisation than an increase in mean annual temperature. This assumption results from the presented transition from snowmelt into glacier melt during the summer half-year. As the Westerlies provide a significant amount of precipitation until late in spring, snowmelt could already decimate snow stocks before the main precipitation supply stops. This would result in an elongated melting period and probably less pronounced peak discharge events (because snow stocks might be empty), which could reduce the risk of floods

ESURFD

2, 1155–1215, 2014

Hydrological cycle of the Central Pamirs

E. Pohl et al.

Title Page

Abstract | Introduction

Conclusions | References

Tables | Figures

⏮ | ⏭

◀ | ▶

Back | Close

Full Screen / Esc

Printer-friendly Version

Interactive Discussion

(cf. Kure et al., 2013). On the other hand, an increase of liquid precipitation provided on existing snow cover bares an increased avalanche risk (Hägeli and McClung, 2003; Zischg et al., 2005). Due to the strong temperature–discharge relationship (Fig. 8f), the most influential precursors leading to floods at the moment are winter precipitation (re-sulting in large snow stocks) and abrupt increases in temperature (triggering the melt). More liquid precipitation as it is e.g. the case with TRMM does not necessarily result in more discharge, but might simply result in more evapotranspiration. A better under-standing of such short-term meteorological variabilities is therefore strongly needed.

About 30 % of the annual discharge results from glacier melt in summer. Negative glacier mass balances of $\approx -0.6\,\mathrm{m\,w.e.\,yr^{-1}}$ point to a potential diminution of glaciers that would consequently have a strong impact on hydropower and agriculture down-stream. In combination with a sooner onset of the melting season, water availability would change in amount and temporal distribution which will demand adapted agri-cultural strategies. It is unclear whether and how much climate change will affect the distribution of Westerlies- or ISM-induced precipitation and their effect on the hydrolog-ical cycle in the Pamirs. This is to a large extent the result of lacking data, both accurate spatially distributed datasets and validation data to prevent inaccurate analyses.

Last, the presented approach will allow new insights to a range of interdisciplinary studies, e.g. on landscape evolution by providing high spatiotemporal resolution data as basis to deepen our understanding of climate/weather variability impacts on erosional processes (e.g. DiBiase and Whipple, 2011; Champagnac et al., 2012; Dietrich et al., 1992; Iverson, 2000; Montgomery and Brandon, 2002). It also sheds some light on the very unusual discrepancy between erosion and incision rates in the Pamir (Fuchs et al., 2013, 2014).

Hydrological cycle of the Central Pamirs

E. Pohl et al.

Title Page

Abstract	Introduction
Conclusions	References
Tables	Figures

Back | Close

Full Screen / Esc

Printer-friendly Version

Interactive Discussion

Appendix A

Relative humidity was calculated based on GLDAS_NOAH025SUBP_3H vapour pressures and temperatures according to the formulas provided via Email by the LP DAAC:

$$MR = \frac{SH}{1 - SH} \tag{A1}$$

$$E_a = \frac{p \times MR}{MR + 0.622} \tag{A2}$$

$$E_s = 611.2 \exp\frac{17.67 \times T}{T + 243.5} \tag{A3}$$

$$RH = E_a/E_s \times 100 \tag{A4}$$

where SH is the specific humidity in $kg\,kg^{-1}$, MR is the mixing ratio, E_a is the actual vapour pressure in Pa, p is the atmospheric pressure in Pa, E_s is the saturated vapor pressure in Pa, T is the temperature in °C, and RH is the relative humidity in %. The equations were directly implemented into the script, extracting the data.

Title Page

Abstract | Introduction

Conclusions | References

Tables | Figures

◄ | ►

◄ | ►

Back | Close

Full Screen / Esc

Printer-friendly Version

Interactive Discussion

References

Ad-hoc-Arbeitsgruppe Boden: Bodenkundliche Kartieranleitung, 5th Edn., Bundesanstalt für Geowissenschaften und Rohstoffe in Zusammenarbeit mit den Staatlichen Geologischen Diensten, Hannover, 2005. 1166, 1167

Agakhanyantz, O. E. and Lopatin, I. K.: Main characteristics of the ecosystems of the Pamirs, USSR, Arctic Alpine Res., 10, 397–407, doi:10.2307/1550770, 1978. 1167

Aizen, V. B., Mayewski, P. A., Aizen, E. M., Joswiak, D. R., Surazakov, A. B., Kaspari, S., Grigholm, B., Krachler, M., Handley, M., and Finaev, A.: Stable-isotope and trace element time series from Fedchenko glacier (Pamirs) snow/firn cores, J. Glaciol., 55, 275–291, doi:10.3189/002214309788608787, 2009. 1158, 1161

Allen, R. G., Pereira, L. S., Raes, D., and Smith, M.: Crop Evapotranspiration – Guidelines for Computing Crop Water Requirements, 56th edn., FAO – Food and Agriculture Organization of the United Nations, Rome, 1998. 1164

Andermann, C., Bonnet, S., and Gloaguen, R.: Evaluation of precipitation data sets along the Himalayan front, Geochem. Geophy. Geosy., 12, Q07023, doi:10.1029/2011GC003513, 2011. 1170

Andermann, C., Bonnet, S., Crave, A., Davy, P., Longuevergne, L., and Gloaguen, R.: Sediment transfer and the hydrological cycle of Himalayan rivers in Nepal, CR Geosci., 344, 627–635, doi:10.1016/j.crte.2012.10.009, 2012a. 1187

Andermann, C., Longuevergne, L., Bonnet, S., Crave, A., Davy, P., and Gloaguen, R.: Impact of transient groundwater storage on the discharge of Himalayan rivers, Nat. Geosci., 5, 127–132, doi:10.1038/ngeo1356, 2012b. 1181, 1183

Awange, J., Fleming, K., Kuhn, M., Featherstone, W., Heck, B., and Anjasmara, I.: On the suitability of the 4° × 4° GRACE mascon solutions for remote sensing Australian hydrology, Remote Sens. Environ., 115, 864–875, doi:10.1016/j.rse.2010.11.014, 2011. 1160

Batu, V.: Aquifer Hydraulics: a Comprehensive Guide to Hydrogeologic Data Analysis, John Wiley & Sons, Inc., Hoboken, NJ, USA, 1998. 1168

Bookhagen, B. and Burbank, D. W.: Toward a complete Himalayan hydrological budget: spatiotemporal distribution of snowmelt and rainfall and their impact on river discharge, J. Geophys. Res., 115, 1–25, doi:10.1029/2009JF001426, 2010. 1158, 1160, 1169, 1183, 1184

Breckle, S. W. and Wucherer, W.: Vegetation of the Pamir (Tajikistan), in: Land Use Change and Mountain Biodiversity, edited by: Spehn, E. M., Körner, C., and Liberman, M., chap. 16, CRC Press, Boca Raton, FL, USA, doi:10.1201/9781420002874.ch16, 225–237, 2006. 1167

Breuer, L. and Frede, H.: PlaPaDa – an online plant parameter data drill for eco-hydrological modelling approaches, available at: http://www.uni-giessen.de/~gh1461/plapada/plapada.html (last access: 10 December 2014), 2003. 1167

Burbank, D. W., Blythe, A. E., Putkonen, J., Pratt-Situala, B., Gabet, E., Oskin, M., Barros, A., and Ojha, T. P.: Decoupling of erosion and precipitation in the Himalayas, Nature, 426, 652–655, doi:10.1038/nature02187, 2003. 1187

Champagnac, J.-D., Molnar, P., Sue, C., and Herman, F.: Tectonics, climate, and mountain topography, J. Geophys. Res., 117, B02403, doi:10.1029/2011JB008348, 2012. 1159, 1189

Chen, F. and Dudhia, J.: Coupling an Advanced Land Surface–Hydrology Model with the Penn State–NCAR MM5 Modeling System. Part I: Model implementation and sensitivity, Mon. Weather Rev., 129, 569–585, doi:10.1175/1520-0493(2001)129<0569:CAALSH>2.0.CO;2, 2001. 1173

Chen, F., Manning, K. W., LeMone, M. A., Trier, S. B., Alfieri, J. G., Roberts, R., Tewari, M., Niyogi, D., Horst, T. W., Oncley, S. P., Basara, J. B., and Blanken, P. D.: Description and evaluation of the characteristics of the NCAR High-Resolution Land Data Assimilation System, J. Appl. Meteorol. Clim., 46, 694–713, doi:10.1175/JAM2463.1, 2007. 1173

Cooper, H. J., Lanier, R. J., Fuelberg, H. E., and Watson, A. I.: Comparing the operational capabilities of the site specific hydrologic predictor (SSHP) and a fully distributed hydrological model (MIKE SHE) using WSR-88 radar rainfall inputs over a small basin in Florida, in: 20th Conference on Hydrology, Atlanta, GA, 28 January–2 February 2006, Amer. Meteor. Soc, available at: http://ams.confex.com/ams/Annual2006/techprogram/session_19002.htm (last access: 10 December 2014), 2006. 1163

Daniel, E. B.: Watershed modeling and its applications: a state-of-the-art review, Open Hydrol. J., 5, 26–50, doi:10.2174/1874378101105010026, 2011. 1162

Dee, D. P., Uppala, S. M., Simmons, A. J., Berrisford, P., Poli, P., Kobayashi, S., Andrae, U., Balmaseda, M. A., Balsamo, G., Bauer, P., Bechtold, P., Beljaars, A. C. M., van de Berg, L., Bidlot, J., Bormann, N., Delsol, C., Dragani, R., Fuentes, M., Geer, A. J., Haimberger, L., Healy, S. B., Hersbach, H., Hólm, E. V., Isaksen, L., Kållberg, P., Köhler, M., Matricardi, M., McNally, A. P., Monge-Sanz, B. M., Morcrette, J.-J., Park, B.-K., Peubey, C., de Rosnay, P., Tavolato, C., Thépaut, J.-N., and Vitart, F.: The ERA-Interim reanalysis: configuration and

Hydrological cycle of the Central Pamirs

E. Pohl et al.

performance of the data assimilation system, Q. J. Roy. Meteor. Soc., 137, 553–597, doi:10.1002/qj.828, 2011. 1174

Deus, D., Gloaguen, R., and Krause, P.: Water balance modeling in a semi-arid environment with limited in situ data using remote sensing in Lake Manyara, East African Rift, Tanzania, Remote Sens., 5, 1651–1680, doi:10.3390/rs5041651, 2013. 1160, 1163, 1172

DiBiase, R. A. and Whipple, K. X.: The influence of erosion thresholds and runoff variability on the relationships among topography, climate, and erosion rate, J. Geophys. Res., 116, F04036, doi:10.1029/2011JF002095, 2011. 1159, 1189

Dietrich, W. E., Wilson, C. J., Montgomery, D. R., McKean, J., and Bauer, R.: Erosion thresholds and land surface morphology, Geology, 20, 675–679, 1992. 1187, 1189

Duan, Q., Sorooshian, S., and Gupta, V.: Optimal use of the SCE-UA global optimization method for calibrating watershed models, J. Hydrol., 158, 265–284, doi:10.1016/0022-1694(94)90057-4, 1994. 1174

Ek, M. B., Mitchell, K. E., Lin, Y., Rogers, E., Grunmann, P., Koren, V., Gayno, G., and Tarpley, J. D.: Implementation of Noah land surface model advances in the National Centers for Environmental Prediction operational mesoscale Eta model, J. Geophys. Res., 108, 1–16, doi:10.1029/2002JD003296, 2003. 1173

FAO, IIASA, ISRIC, ISSCAS, and JRC: Harmonized World Soil Database (version 1.1), FAO, Rome, Italy and IIASA, Laxenburg, Austria, 2009. 1166

Fischer, C., Kralisch, S., Krause, P., Fink, M., and Flügel, W.: Calibration of hydrological model parameters with the JAMS framework, in: 18th World IMACS / MODSIM Congress, edited by: Anderssen, R. S., Braddock, R. D., and Newham, L. T. H., July, 866–872, Cairns, Australia, 13–17 July, 2009, available at: http://mssanz.org.au/modsim09 (last access: 10 December 2014), 2009. 1174

Fuchs, M. C., Gloaguen, R., and Pohl, E.: Tectonic and climatic forcing on the Panj river system during the Quaternary, Int. J. Earth Sci., 102, 1985–2003, doi:10.1007/s00531-013-0916-2, 2013. 1158, 1161, 1184, 1187, 1189, 1206

Fuchs, M. C., Gloaguen, R., Merchel, S., Pohl, E., and Sulaymonova, V. A.: Millennial erosion rates across the Pamir based on 10 Be concentrations in fluvial sediments: Dominance of topographic over climatic factors, Earth Surf. Dynam. Discuss., in press, 2014. 1159, 1187, 1189

Gardelle, J., Berthier, E., and Arnaud, Y.: Slight mass gain of Karakoram glaciers in the early twenty-first century, Nat. Geosci., 5, 322–325, doi:10.1038/ngeo1450, 2012. 1160

Hydrological cycle of the Central Pamirs

E. Pohl et al.

Title Page

Abstract	Introduction
Conclusions	References
Tables	Figures

|◄ | ►|

◄ | ►

Back | Close

Full Screen / Esc

Printer-friendly Version

Interactive Discussion

Gardelle, J., Berthier, E., Arnaud, Y., and Kääb, A.: Region-wide glacier mass balances over the Pamir-Karakoram-Himalaya during 1999–2011, The Cryosphere, 7, 1263–1286, doi:10.5194/tc-7-1263-2013, 2013. 1158, 1160, 1183

Godard, V., Bourles, D. L., Spinabella, F., Burbank, D. W., Bookhagen, B., Fisher, G. B., Moulin, A., and Leanni, L.: Dominance of tectonics over climate in Himalayan denudation, Geology, 42, 243–246, doi:10.1130/G35342.1, 2014. 1159

Gruber, F. E. and Mergili, M.: Regional-scale analysis of high-mountain multi-hazard and risk indicators in the Pamir (Tajikistan) with GRASS GIS, Nat. Hazards Earth Syst. Sci., 13, 2779–2796, doi:10.5194/nhess-13-2779-2013, 2013. 1186, 1188

Häckel, H.: Meteorologie, UTB: Geowissenschaften, Agrarwissenschaften, 5th edn., Ulmer UTB, Stuttgart, 1999. 1173

Hägeli, P. and McClung, D. M.: Avalanche characteristics of a transitional snow climate – Columbia Mountains, British Columbia, Canada, Cold Reg. Sci. Technol., 37, 255–276, doi:10.1016/S0165-232X(03)00069-7, 2003. 1189

Hagg, W., Braun, L., Kuhn, M., and Nesgaard, T.: Modelling of hydrological response to climate change in glacierized Central Asian catchments, J. Hydrol., 332, 40–53, doi:10.1016/j.jhydrol.2006.06.021, 2007. 1158

Hagg, W., Hoelzle, M., Wagner, S., Mayr, E., and Klose, Z.: Glacier and runoff changes in the Rukhk catchment, upper Amu-Darya basin until 2050, Global Planet. Change, 110, 62–73, doi:10.1016/j.gloplacha.2013.05.005, 2013. 1158

Haritashya, U. K., Bishop, M. P., Shroder, J. F., Bush, A. B. G., and Bulley, H. N. N.: Space-based assessment of glacier fluctuations in the Wakhan Pamir, Afghanistan, Climatic Change, 94, 5–18, doi:10.1007/s10584-009-9555-9, 2009. 1183

Herman, F., Seward, D., Valla, P. G., Carter, A., Kohn, B., Willett, S. D., and Ehlers, T. A.: Worldwide acceleration of mountain erosion under a cooling climate, Nature, 504, 423–426, doi:10.1038/nature12877, 2013. 1159

Hock, R.: Temperature index melt modelling in mountain areas, J. Hydrol., 282, 104–115, doi:10.1016/S0022-1694(03)00257-9, 2003. 1185

Huffman, G. J.: Estimates of root-mean-square random error for finite samples of estimated precipitation, J. Appl. Meteorol., 36, 1191–1201, doi:10.1175/1520-0450(1997)036<1191:EORMSR>2.0.CO;2, 1997. 1169

Huffman, G. J., Adler, R. F., Arkin, P., Chang, A., Ferraro, R., Gruber, A., Janowiak, J., McNab, A., Rudolf, B., and Schneider, U.: The Global Precipitation Climatology Project

Title Page

Abstract | Introduction

Conclusions | References

Tables | Figures

◄◄ | ►►

◄ | ►

Back | Close

Full Screen / Esc

Printer-friendly Version

Interactive Discussion

(GPCP) combined precipitation dataset, B. Am. Meteorol. Soc., 78, 5–20, doi:10.1175/1520-0477(1997)078<0005:TGPCPG>2.0.CO;2, 1997. 1169

Huffman, G. J., Adler, R. F., Bolvin, D. T., Gu, G., Nelkin, E. J., Bowman, K. P., Hong, Y., Stocker, E. F., and Wolff, D. B.: The TRMM Multisatellite Precipitation Analysis (TMPA): quasi-global, multiyear, combined-sensor precipitation estimates at fine scales, J. Hydrometeorol., 8, 38, doi:10.1175/JHM560.1, 2007. 1169

Hydrological Sciences Branch at NASA/Goddard Space Flight Center (GSFC/HSB): GLDAS Noah Land Surface Model L4 3 Hourly 0.25 × 0.25 degree Subsetted, Goddard Earth Sciences Data and Information Services Center (GES DISC), Greenbelt, Maryland, USA, available at: http://mirador.gsfc.nasa.gov/collections/GLDAS_NOAH025SUBP_3H__001.shtml (last access: 10 December 2014), 2007. 1173

Immerzeel, W., Droogers, P., de Jong, S., and Bierkens, M.: Large-scale monitoring of snow cover and runoff simulation in Himalayan river basins using remote sensing, Remote Sens. Environ., 113, 40–49, doi:10.1016/j.rse.2008.08.010, 2009. 1158, 1162, 1167, 1183, 1184

Immerzeel, W. W., Pellicciotti, F., and Bierkens, M. F. P.: Rising river flows throughout the twenty-first century in two Himalayan glacierized watersheds, Nat. Geosci., 6, 742–745, doi:10.1038/ngeo1896, 2013. 1188

Immerzeel, W. W., Petersen, L., Ragettli, S., and Pellicciotti, F.: The importance of observed gradients of air temperature and precipitation for modeling runoff from a glacierized watershed in the Nepalese Himalayas, Water Resour. Res., 50, 2212–2226, doi:10.1002/2013WR014506, 2014. 1159

Iverson, R. M.: Landslide triggering by rain infiltration, Water Resour. Res., 36, 1897–1910, doi:10.1029/2000WR900090, 2000. 1187, 1189

Jarvis, A., Reuter, H., and Nelson, A.: Hole-filled seamless SRTM data V4, available at: srtm.csi.cgiar.org (last access: 10 December 2014), 2008. 1166

Kamal-Heikman, S., Derry, L. A., Stedinger, J. R., and Duncan, C. C.: A simple predictive tool for lower Brahmaputra River Basin monsoon flooding, Earth Interact., 11, 1–11, doi:10.1175/EI226.1, 2007. 1169, 1170, 1185

Kawashima, S., Ishida, T., Minomura, M., and Miwa, T.: Relations between surface temperature and air temperature on a local scale during winter nights, J. Appl. Meteorol., 39, 1570–1579, doi:10.1175/1520-0450(2000)039<1570:RBSTAA>2.0.CO;2, 2000. 1172

Khan, S. I., Adhikari, P., Hong, Y., Vergara, H., F Adler, R., Policelli, F., Irwin, D., Korme, T., and Okello, L.: Hydroclimatology of Lake Victoria region using hydrologic model and satellite

ESURFD

2, 1155–1215, 2014

Hydrological cycle of the Central Pamirs

E. Pohl et al.

Title Page

Abstract	Introduction
Conclusions	References
Tables	Figures

◄◄   ►►

◄   ►

Back   Close

Full Screen / Esc

Printer-friendly Version

Interactive Discussion

remote sensing data, Hydrol. Earth Syst. Sci., 15, 107–117, doi:10.5194/hess-15-107-2011, 2011. 1160, 1163

Khromova, T., Osipova, G., Tsvetkov, D., Dyurgerov, M., and Barry, R.: Changes in glacier extent in the eastern Pamir, Central Asia, determined from historical data and ASTER imagery, Remote Sens. Environ., 102, 24–32, doi:10.1016/j.rse.2006.01.019, 2006. 1183

Kralisch, S., Krause, P., Fink, M., Fischer, C., and Flügel, W.: Component based environmental modelling using the JAMS framework, in: Proceedings of MODSIM07, edited by: Oxley, L., and Kulasiri, D., 812–818, Modelling and Simulation Society of Australia and New Zealand, Christchurch, New Zealand, available at: http://www.mssanz.org.au/MODSIM07/papers/14_s51/ComponentBasedEnvironmenta_s51_Kralisch_l.pdf (last access: 10 December 2014), 2007. 1163

Krause, P. and Hanisch, S.: Simulation and analysis of the impact of projected climate change on the spatially distributed waterbalance in Thuringia, Germany, Adv. Geosci., 21, 33–48, doi:10.5194/adgeo-21-33-2009, 2009. 1163

Krause, P., Biskop, S., Helmschrot, J., Flügel, W.-A., Kang, S., and Gao, T.: Hydrological system analysis and modelling of the Nam Co basin in Tibet, Adv. Geosci., 27, 29–36, doi:10.5194/adgeo-27-29-2010, 2010. 1163

Kure, S., Jang, S., Ohara, N., Kavvas, M. L., and Chen, Z. Q.: Hydrologic impact of regional climate change for the snowfed and glacierfed river basins in the Republic of Tajikistan: hydrological response of flow to climate change, Hydrol. Process., 27, 4057–4070, doi:10.1002/hyp.9535, 2013. 1158, 1188, 1189

Liu, T., Willems, P., Feng, X. W., Li, Q., Huang, Y., Bao, A. M., Chen, X., Veroustraete, F., and Dong, Q. H.: On the usefulness of remote sensing input data for spatially distributed hydrological modelling: case of the Tarim River basin in China, Hydrol. Process., 26, 335–344, doi:10.1002/hyp.8129, 2012. 1160, 1163

Lutz, A. F., Immerzeel, W. W., Gobiet, A., Pellicciotti, F., and Bierkens, M. F. P.: Comparison of climate change signals in CMIP3 and CMIP5 multi-model ensembles and implications for Central Asian glaciers, Hydrol. Earth Syst. Sci., 17, 3661–3677, doi:10.5194/hess-17-3661-2013, 2013. 1158, 1159, 1183

Lutz, A. F., Immerzeel, W. W., Shrestha, A. B., and Bierkens, M. F. P.: Consistent increase in High Asia's runoff due to increasing glacier melt and precipitation, Nat. Clim. Change, 4, 587–592, doi:10.1038/nclimate2237, 2014. 1158, 1160, 1170, 1183, 1185

Title Page

Abstract | Introduction

Conclusions | References

Tables | Figures

|◄ | ►|

◄ | ►

Back | Close

Full Screen / Esc

Printer-friendly Version

Interactive Discussion

Maussion, F., Scherer, D., Finkelnburg, R., Richters, J., Yang, W., and Yao, T.: WRF simulation of a precipitation event over the Tibetan Plateau, China – an assessment using remote sensing and ground observations, Hydrol. Earth Syst. Sci., 15, 1795–1817, doi:10.5194/hess-15-1795-2011, 2011. 1171, 1172

Maussion, F., Scherer, D., Mölg, T., Collier, E., Curio, J., and Finkelnburg, R.: Precipitation seasonality and variability over the Tibetan Plateau as resolved by the High Asia Reanalysis, J. Climate, 27, 1910–1927, doi:10.1175/JCLI-D-13-00282.1, 2014. 1160, 1170

Ménégoz, M., Gallée, H., and Jacobi, H. W.: Precipitation and snow cover in the Himalaya: from reanalysis to regional climate simulations, Hydrol. Earth Syst. Sci., 17, 3921–3936, doi:10.5194/hess-17-3921-2013, 2013. 1159, 1168, 1184

Merritt, W., Alila, Y., Barton, M., Taylor, B., Cohen, S., and Neilsen, D.: Hydrologic response to scenarios of climate change in sub watersheds of the Okanagan basin, British Columbia, J. Hydrol., 326, 79–108, doi:10.1016/j.jhydrol.2005.10.025, 2006. 1163

Mischke, S., Rajabov, I., Mustaeva, N., Zhang, C., Herzschuh, U., Boomer, I., Brown, E. T., Andersen, N., Myrbo, A., and Ito, E.: Modern hydrology and late Holocene history of Lake Karakul, eastern Pamirs (Tajikistan): a reconnaissance study, Palaeogeogr. Palaeocl., 289, 10–24, doi:10.1016/j.palaeo.2010.02.004, 2010. 1158, 1161

Mölg, T., Maussion, F., and Scherer, D.: Mid-latitude westerlies as a driver of glacier variability in monsoonal High Asia, Nature Climate Change, 4, 68–73, doi:10.1038/nclimate2055, 2013. 1171, 1172, 1185

Montgomery, D. R. and Brandon, M. T.: Topographic controls on erosion rates in tectonically active mountain ranges, Earth Planet. Sc. Lett., 201, 481–489, doi:10.1016/S0012-821X(02)00725-2, 2002. 1159, 1189

Mostovoy, G. V., King, R. L., Reddy, K. R., Kakani, V. G., and Filippova, M. G.: Statistical estimation of daily maximum and minimum air temperatures from MODIS LST data over the State of Mississippi, GISci. Remote Sens., 43, 78–110, 2006. 1172

Mu, Q., Zhao, M., and Running, S. W.: Improvements to a MODIS global terrestrial evapotranspiration algorithm, Remote Sens. Environ., 115, 1781–1800, doi:10.1016/j.rse.2011.02.019, 2011. 1184

Narzikulov, I. K. and Stanjukovič, K. V.: Atlas Tadzikskoj Sovetskoj Socialisticeskoj Respubliki, Akademija Nauk Tadžikskoj SSR, Dušanbe Sovet po Izučeniju Proizvoditel'nych Sil, Moskau, Dušanbe, 1968. 1166, 1168

Title Page

Abstract | Introduction

Conclusions | References

Tables | Figures

◄◄ | ►►

◄ | ►

Back | Close

Full Screen / Esc

Printer-friendly Version

Interactive Discussion

Nash, J. and Sutcliffe, J.: River flow forecasting through conceptual models part I – A discussion of principles, J. Hydrol., 10, 282–290, doi:10.1016/0022-1694(70)90255-6, 1970. 1174

National Centers for Environmental Prediction NOAA, US Department of Commerce, N. W. S.: NCEP FNL Operational Model Global Tropospheric Analyses, continuing from July 1999, Research Data Archive at the National Center for Atmospheric Research, Computational and Information Systems Laboratory, Boulder, CO, doi:10.5065/D6M043C6, 2000. 1171

Nepal, S., Krause, P., Flügel, W.-A., Fink, M., and Fischer, C.: Understanding the hydrological system dynamics of a glaciated alpine catchment in the Himalayan region using the J2000 hydrological model, Hydrol. Process., 28, 1329–1344, doi:10.1002/hyp.9627, 2014. 1163

Ollesch, G., Sukhanovski, Y., Kistner, I., Rode, M., and Meissner, R.: Characterization and modelling of the spatial heterogeneity of snowmelt erosion, Earth Surf. Proc. Land., 211, 197–211, doi:10.1002/esp.1175, 2005. 1187

Ollesch, G., Kistner, I., Meissner, R., and Lindenschmidt, K.-E.: Modelling of snowmelt erosion and sediment yield in a small low-mountain catchment in Germany, Catena, 68, 161–176, doi:10.1016/j.catena.2006.04.005, 2006. 1187

Palazzi, E., Hardenberg, J. V., and Provenzale, A.: Precipitation in the Hindu-Kush Karakoram Himalaya: observations and future scenarios, J. Geophys. Res.-Atmos., 118, 85–100, 2013. 1158, 1159, 1161, 1168

Peel, M. C., Finlayson, B. L., and McMahon, T. A.: Updated world map of the Köppen-Geiger climate classification, Hydrol. Earth Syst. Sci., 11, 1633–1644, doi:10.5194/hess-11-1633-2007, 2007. 1162

Prigent, C.: Precipitation retrieval from space: an overview, CR Geosci., 342, 380–389, doi:10.1016/j.crte.2010.01.004, 2010. 1160, 1169, 1185

Pu, Z., Xu, L., and Salomonson, V. V.: MODIS/Terra observed seasonal variations of snow cover over the Tibetan Plateau, Geophys. Res. Lett., 34, L06706, doi:10.1029/2007GL029262, 2007. 1162, 1184

R Core Team: R: A Language and Environment for Statistical Computing, R Foundation for Statistical Computing, Vienna, Austria, available at: http://www.r-project.org (last access: 10 December 2014), 2014. 1165, 1172

Rodell, M., Houser, P. R., Jambor, U., Gottschalck, J., Mitchell, K., Meng, C. J., Arsenault, K., Cosgrove, B., Radakovich, J., Bosilovich, M., Entin, J. K., Walker, J. P., Lohmann, D., and Toll, D.: The global land data assimilation system, B. Am. Meteorol. Soc., 85, 381, doi:10.1175/BAMS-85-3-381, 2004. 1173

Roe, G. H.: Orographic precipitation, Annu. Rev. Earth Pl. Sc., 33, 645–671, doi:10.1146/annurev.earth.33.092203.122541, 2005. 1169

Samaniego, L., Kumar, R., and Jackisch, C.: Predictions in a data-sparse region using a regionalized grid-based hydrologic model driven by remotely sensed data, Hydrol. Res., 42, 338–355, doi:10.2166/nh.2011.156, 2011. 1160

Scherler, D., Bookhagen, B., and Strecker, M. R.: Tectonic control on 10 Be-derived erosion rates in the Garhwal Himalaya, India, J. Geophys. Res.-Earth, 119, 83–105, doi:10.1002/2013JF002955, 2014. 1187

Schwarze, R., Dröge, W., and Opherden, K.: Regional analysis and modelling of groundwater runoff components from catchments in hard rock areas, in: Regionalization in Hydrology, edited by: Diekkrüger, B., Kirkby, M. J., and Schröder, U., 221–232, International Association of Hydroiogical Sciences, Braunschweig, 1999. 1183

Skamarock, W. C. and Klemp, J. B.: A time-split nonhydrostatic atmospheric model for weather research and forecasting applications, J. Comput. Phys., 227, 3465–3485, doi:10.1016/j.jcp.2007.01.037, 2008. 1171

Skofronick-Jackson, G. and Weinman, J.: A physical model to determine snowfall over land by microwave radiometry, IEEE T. Geosci. Remote, 42, 1047–1058, doi:10.1109/TGRS.2004.825585, 2004. 1170, 1185

Sorg, A., Bolch, T., Stoffel, M., Solomina, O., and Beniston, M.: Climate change impacts on glaciers and runoff in Tien Shan (Central Asia), Nature Climate Change, 2, 725–731, doi:10.1038/nclimate1592, 2012. 1159, 1160, 1184

Stahl, K., Moore, R. D., Shea, J. M., Hutchinson, D., and Cannon, A. J.: Coupled modelling of glacier and streamflow response to future climate scenarios, Water Resour. Res., 44, W02422, doi:10.1029/2007WR005956, 2008. 1163

Strahler, A., Muchoney, D., Borak, J., Friedl, M., Gopal, S., Lambin, E., and Moody, A.: MODIS Land Cover Product Algorithm Theoretical Basis Document (ATBD) MODIS Land Cover and Land-Cover Change, available at: http://modis.gsfc.nasa.gov/data/atbd/atbd_mod12.pdf (last access: 10 December 2014), 1999. 1167

Syed, F. S., Giorgi, F., Pal, J. S., and King, M. P.: Effect of remote forcings on the winter precipitation of central southwest Asia part 1: observations, Theor. Appl. Climatol., 86, 147–160, doi:10.1007/s00704-005-0217-1, 2006. 1158, 1161

Hydrological cycle of the Central Pamirs

E. Pohl et al.

Tahir, A. A., Chevallier, P., Arnaud, Y., and Ahmad, B.: Snow cover dynamics and hydrological regime of the Hunza River basin, Karakoram Range, Northern Pakistan, Hydrol. Earth Syst. Sci., 15, 2275–2290, doi:10.5194/hess-15-2275-2011, 2011. 1158

Takala, M., Luojus, K., Pulliainen, J., Derksen, C., Lemmetyinen, J., Kärnä, J.-P., Koskinen, J., and Bojkov, B.: Estimating northern hemisphere snow water equivalent for climate research through assimilation of space-borne radiometer data and ground-based measurements, Remote Sens. Environ., 115, 3517–3529, doi:10.1016/j.rse.2011.08.014, 2011. 1160

Tong, J., Dery, S. J., Jackson, P. L., and Derksen, C.: Testing snow water equivalent retrieval algorithms for passive microwave remote sensing in an alpine watershed of western Canada, Can. J. Remote Sens., 36, 74–86, 2010. 1160

Tustison, B., Harris, D., and Foufoula-Georgiou, E.: Scale issues in verification of precipitation forecasts, J. Geophys. Res.-Atmos., 106, 11775–11784, doi:10.1029/2001JD900066, 2001. 1160, 1168

Wan, Z.: New refinements and validation of the MODIS land-surface temperature/emissivity products, Remote Sens. Environ., 112, 59–74, doi:10.1016/j.rse.2006.06.026, 2008. 1172

Wan, Z. and Li, Z.-L.: A physics-based algorithm for retrieving land-surface emissivity and temperature from EOS/MODIS data, IEEE T. Geosci. Remote, 35, 980–996, doi:10.1109/36.602541, 1997. 1172

Wan, Z., Zhang, Y., Zhang, Q., and Li, Z. L.: Quality assessment and validation of the MODIS global land surface temperature, Int. J. Remote Sens., 25, 261–274, doi:10.1080/0143116031000116417, 2004. 1172

Wood, A. W., Leung, L. R., Sridhar, V., and Lettenmaier, D. P.: Hydrologic implications of dynamical and statistical approaches to downscaling climate model outputs, Climatic Change, 62, 189–216, doi:10.1023/B:CLIM.0000013685.99609.9e, 2004. 1159, 1163

Xiao, X., Moore, B., Qin, X., Shen, Z., and Boles, S.: Large-scale observations of alpine snow and ice cover in Asia: using multi-temporal VEGETATION sensor data, Int. J. Remote Sens., 23, 2213–2228, doi:10.1080/01431160110076180, 2002. 1158, 1162, 1184

Yatagai, A., Arakawa, O., Kamiguchi, K., and Kawamoto, H.: A 44-year daily gridded precipitation dataset for Asia, SOLA, 5, 137–140, doi:10.2151/sola.2009-035, 2009. 1170

Yatagai, A., Kamiguchi, K., Arakawa, O., Hamada, A., Yasutomi, N., and Kitoh, A.: APHRODITE: constructing a long-term daily gridded precipitation dataset for Asia based on a dense network of rain gauges, B. Am. Meteorol. Soc., 93, 1401–1415, doi:10.1175/BAMS-D-11-00122.1, 2012. 1170

Title Page

Abstract | Introduction

Conclusions | References

Tables | Figures

|◀ | ▶|

◀ | ▶

Back | Close

Full Screen / Esc

Printer-friendly Version

Interactive Discussion

Yin, Z.-Y.: Using a geographic information system to improve special sensor microwave imager precipitation estimates over the Tibetan Plateau, J. Geophys. Res., 109, D03110, doi:10.1029/2003JD003749, 2004. 1170, 1185

Zech, R., Abramowski, U., Glaser, B., Sosin, P., Kubik, P., and Zech, W.: Late quaternary glacial and climate history of the Pamir Mountains derived from cosmogenic be exposure ages, Quaternary Res., 64, 212–220, doi:10.1016/j.yqres.2005.06.002, 2005. 1206

Zischg, A., Fuchs, S., Keiler, M., and Meißl, G.: Modelling the system behaviour of wet snow avalanches using an expert system approach for risk management on high alpine traffic roads, Nat. Hazards Earth Syst. Sci., 5, 821–832, doi:10.5194/nhess-5-821-2005, 2005. 1189

Table 1. Model parameters. All used model parameters included in the optimisation process including their possible value ranges. Parameterisation values apply to all HRUs unless specified differently.

Parameter	Value range	Description
T_{base}	−8 to 8 °C	Threshold temperature for freezing/melting of non-glaciated HRUs
TMF_s	0 to 8 mm °C^{-1} day^{-1}	Degree-day-factor for snowmelt of non-glaciated HRUs
T_{base_g}	−5 to 7 °C	Threshold temperature for freezing/melting of glaciated HRUs
TMF_{gs}	0 to 8 mm °C^{-1} day^{-1}	Degree-day-factor for snowmelt of glaciated HRUs
TMF_{gi}	0 to 8 mm °C^{-1} day^{-1}	Degree-day-factor for ice melt of glaciated HRUs
ETR	0 to 0.7	Evapotranspiration reduction factor accounting for increasing resistance against evapotranspiration with decreasing soil moisture content
maxPerc	1E-04 to 20	Scaling factor for maximum percolation rates
LVD	0 to 5	Lateral-Vertical-Distribution; lower values for more vertical and less lateral flow
FCA	0 to 2	Field-Capacity-Adaption; lower values for less field capacity
gwStorAlpha	0 to 1	Distribution coefficient of percolation to either groundwater storage components; lower values for higher contribution to deep groundwater and less contribution to fast recession component
GWK_1	0 to 100	Recession parameter for the first linear storage (fast subsurface flow)
GWK_2	100 to 400	Recession parameter for the second linear storage (deep groundwater)

Discussion Paper | Discussion Paper | Discussion Paper | Discussion Paper |

Table 2. Used input for derivation of HRUs and meteorological input data with specifications about temporal and spatial resolution. For static parameters the date of creation is given if available. SAHT is the State Administration for Hydrometeorology of Tajikistan and HWSD is the Harmonized World Soil Database. For the actual modelling, hourly values were averaged or summed up to yield daily values.

Input	Dataset	Spatial Resolution	Temporal Resolution
Parameter Data			
Elevation, slope, aspect	SRTM DEM	90 m	static (1999)
Land use	MODIS MCD12Q1	500 m	static (2005)
Soil	SAHT map/HWSD	NA/vector map	static (NA/2009 HWSD)
Hydrogeology	SAHT map	NA	static (NA)
Meteorological Data			
Precipitation	TRMM3B42 V7/APHRO_MA_V1101/HAR10	$0.25°/0.25°/\approx 0.10°$	daily
Temperature	MODIS MOD11C1 V5/HAR10	$0.05°/\approx 0.10°$	daily
Wind speed	GLDAS_NOAH025SUBP_3H	$0.25°$	3 hourly
Relative humidity	GLDAS_NOAH025SUBP_3H	$0.25°$	3 hourly
Sunshine duration	ECMWF Era Interim	$0.75°$	12 hourly

Title Page

Abstract | Introduction

Conclusions | References

Tables | Figures

|◀ | ▶|

◀ | ▶

Back | Close

Full Screen / Esc

Printer-friendly Version

Interactive Discussion

Table 3. Precipitation datasets with applied correction factors. APHRO is APHRO_MA_V1101, and TRMM is TRMM3B42 V7. Values inside parenthesis correspond to resulting average annual precipitation amount. HAR10 in its original version provides 688 mm of average annual precipitation and has been downward corrected in a first step to yield a ratio of unity with in situ measurements (the resulting dataset is HAR10 (172 mm).

Dataset Name	Correction Factor
APHRO (152 mm)	1
APHRO (200 mm)	1.3
TRMM (308 mm)	1
TRMM (400 mm)	1.3
HAR10 (172 mm)	1
HAR10 (224 mm)	1.3
HAR10 (258 mm)	1.5

Table 4. Model parameterisations and NSE for the calibration time period 2002 to 2007.

Model Setup	T_{base}	TMF_s	T_{base_g}	TMF_{gs}	TMF_{gi}	ETR	maxPerc	LVD	FCA	gwStorAlpha	GWK_1	GWK_2	RMSE	NSE
MODIS MOD11C1 V5 temperature														
APHRO (154 mm)	6.08	3.77	−4.49	3.87	1.05	0.44	10.37	4.18E-02	4.07E-03	0.72	12.59	339.07	41.05	0.86
APHRO (200 mm)	7.16	6.47	−4.29	3.07	0.86	0.45	5.02	1.69E-02	2.28E-02	0.55	12.50	393.88	36.58	0.89
HAR10 (172 mm)	6.15	3.86	−3.15	1.48	1.04	0.48	9.36	2.46E-02	3.56E-03	0.59	14.47	242.89	38.29	0.88
HAR10 (224 mm)	5.33	3.51	−0.04	3.45	1.18	0.24	8.35	3.19E-03	4.55E-03	0.44	14.66	353.85	33.97	0.90
HAR10 (258 mm)	5.01	4.31	0.96	4.07	0.89	0.45	12.08	1.26E-03	3.56E-02	0.41	19.16	216.49	32.47	0.91
TRMM (308 mm)	4.00	2.63	−0.89	3.76	1.02	0.32	7.60	2.19E-03	1.26E-01	0.34	10.35	287.54	38.80	0.87
TRMM (400 mm)	2.65	5.10	1.22	1.91	1.25	0.65	8.10	2.07E-02	6.01E-01	0.32	15.84	393.98	40.26	0.86
HAR10 temperature														
APHRO (154 mm)	3.82	2.49	−4.86	1.29	0.94	0.14	14.41	2.73E-01	1.97E-02	0.69	14.32	288.64	45.00	0.83
APHRO (200 mm)	2.57	4.85	0.55	3.40	1.19	0.35	12.90	2.54E-03	1.40E-04	0.50	20.55	355.71	41.50	0.86
HAR10 (172 mm)	3.76	6.95	0.18	2.02	1.11	0.35	11.03	2.62E-03	4.37E-04	0.53	21.02	395.76	41.04	0.86
HAR10 (224 mm)	3.46	7.85	1.34	2.80	0.91	0.66	11.64	1.23E-03	4.95E-02	0.54	30.29	399.34	38.25	0.88
HAR10 (258 mm)	3.17	7.08	2.03	3.74	0.72	0.21	2.96	7.96E-04	9.24E-02	0.60	38.61	398.98	37.57	0.88
TRMM (308 mm)	0.45	5.20	0.23	1.08	1.11	0.01	10.30	1.99E-02	1.17E-01	0.42	22.53	263.04	42.91	0.85
TRMM (400 mm)	−0.78	4.97	0.70	1.52	1.21	0.29	10.25	1.75E-03	5.08E-01	0.39	22.27	388.09	43.80	0.84

Figure 1. Study area in the Tajik Pamirs with catchment area of the Gunt and Shakhdara rivers and available meteorological stations and discharge measurement location. Monsoon and Westerlies indicated by arrows according to Zech et al. (2005); Fuchs et al. (2013). MODIS MCD12Q1 land cover class 15 indicating permanent ice and snow cover (lightblue) as proxy for glacier extent.
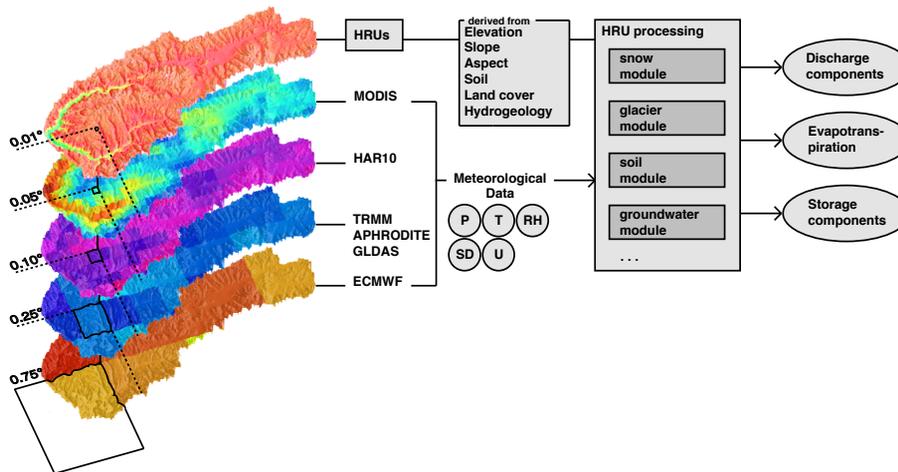
Figure 2. Schematic superimposition of different meteorological raster data with various spatial resolutions. HRUs have 1 km × 1 km pixel size. Processing modules of the J2000g model take needed forcing data (P precipitation, T temperature, RH relative humidity, SD sunshine hours, U near-ground wind speed) to be processed for each individual HRU. Final step is the output of discharge components, evapotranspiration and storage changes.
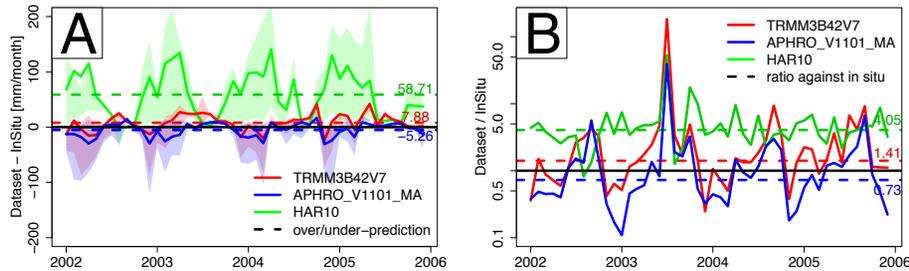
Figure 3. Comparison of precipitation amounts of a particular precipitation dataset with in situ data. Bold lines are mean monthly values for all pixels encompassing meteorological stations. Dashed line is the mean value for the entire period from 2002 to 2006. **(a)** Difference in intensities on a monthly basis. Strong overestimation for HAR10 and underestimation for TRMM3B42 V7, and APHRO_MA_V1101 in winter. Shaded area marks range between minimum and maximum of raster and in situ data. **(b)** Normalised datasets by in situ data show a constant value of ≈ 4 for HAR10 and varying values for TRMM3B42 V7, and APHRO_MA_V1101 (extreme values in summer 2003 due to almost no recorded precipitation events in the in situ dataset.) Note the logarithmic scale.
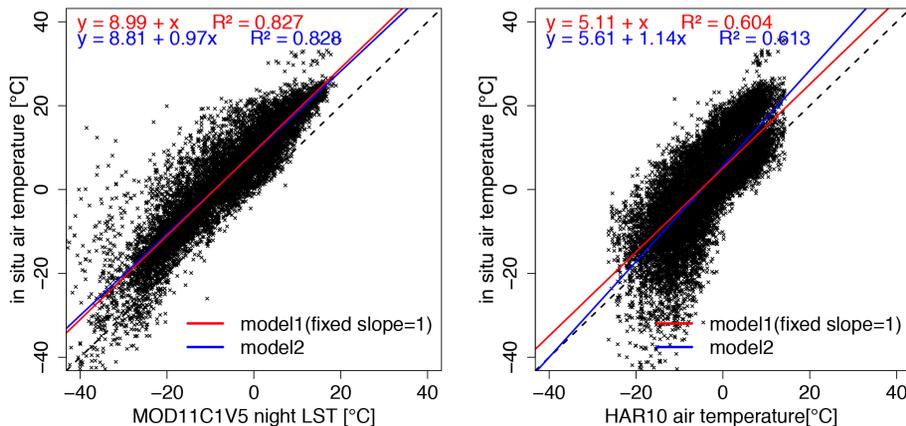
Figure 4. Comparison of MODIS MOD11C1 V5 night LST and HAR10 2 m air temperature with in situ data. Scatterplots represent values for all pixels encompassing a meteorological station providing data. Scattering is actually smaller and correlation is higher when comparison is based on a single pixel and the encompassed meteorological station data. For calibration, the intercept values of the linear models with fixed slope of 1 (red) are added to the original datasets.

Figure 5. Model results for the two different temperature datasets in combination with the individual best performing precipitation dataset. Descending ordering according to best NSE. First panel exemplarily represents the legend. Negligible amounts of Q_{surf} result from the model's treatment of snowmelt water with a recession, which is therefore represented by Q_{bas1} (see Sect. 3.2).

Figure 6. Ranges (shaded areas) for calibration parameters during the last steps of SCE-UA optimisation. Only parameterisations for NSE ≥ 0.82 are considered. Possible value ranges are according to Table 1. Left panel displays realisations with setups using MOD11C1 V5 temperatures and right panel those with HAR10 temperatures. Solid lines represent best performing individual precipitation datasets. PrecSum is the average annual precipitation.

Figure 7. J2000g modelling results. Upper panel shows the individual water components for the overall best performing model setup with MOD11C1 V5 temperature and HAR10 (258 mm). Note different scaling for Q_{bas}/Q_{glac} compared to snowmelt, due to higher magnitude of snowmelt. Lower panel shows observed and modelled hydrographs, and cumulative hydrographs. Displayed range (shaded area) corresponds to different temperature datasets.
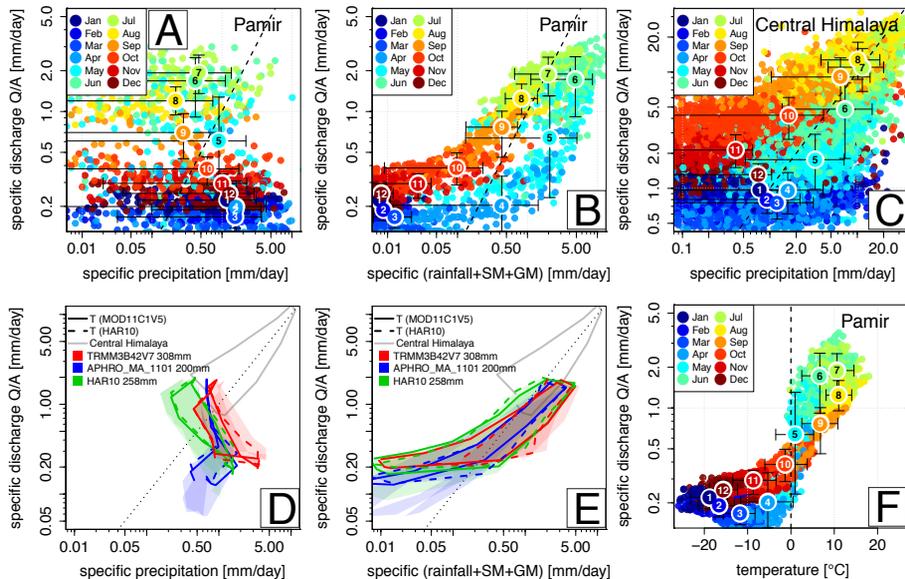
Figure 8. Area-normalised discharge (specific discharge) dependencies on area-normalised precipitation (specific precipitation) and specific effective precipitation P_{eff}, i.e. all liquid water input from rainfall, snowmelt (SM) and glacier melt (GM). All plots on a bi-logarithmic scale except for **(f)**. Modelled discharge (MOD11C1 V5 temperature and HAR10 (258 mm) precipitation) response to **(a)** precipitation and **(b)** P_{eff}. Colour-coding corresponds to month of the year. Error bars represent 95-percentiles and numbers represent mean monthly values. **(d)** and **(e)** include model results from all other model combinations (shaded area) showing the same relationships as **(a)** and **(b)**, respectively; colour-coding corresponds to precipitation datasets. Best individual precipitation datasets with either temperature dataset is represented by the solid or dashed lines. **(c)** shows for comparison purposes the discharge–rainfall relationship for the Naryani Catchment, Central Himalaya, Nepal. The shape is included in **(d)** and **(e)** to highlight similarity in shape but different order of magnitude in both discharge and precipitation. **(f)** displays modelled discharge–temperature relationship.

Title Page

Abstract | Introduction

Conclusions | References

Tables | Figures

|◄ | ►|

◄ | ►

Back | Close

Full Screen / Esc

Printer-friendly Version

Interactive Discussion
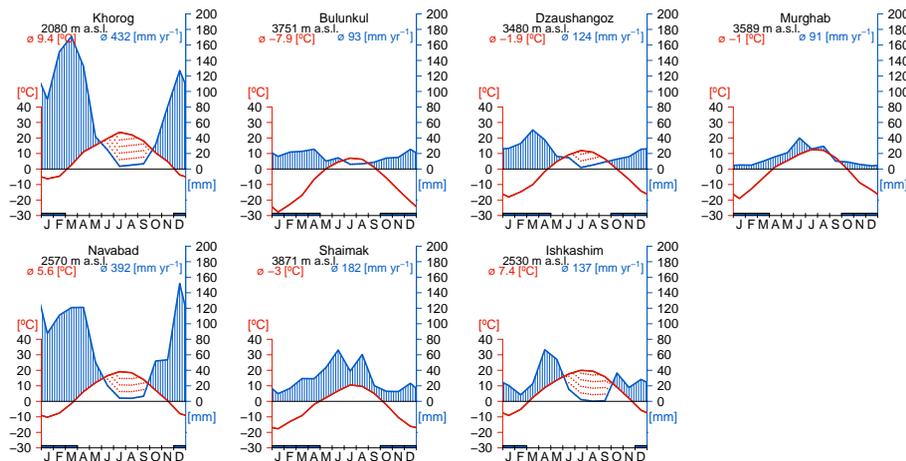
Figure A1. Climate diagrams for the available meteorological stations with precipitation amounts (blue) and temperature (red). Most western stations, Khorog, Navabad, and Ishkashim with distinctive precipitation maximum in winter. Influence of Westerlies in the winter half-year decreases with altitude towards the east (Bulunkul, Murghab, Shaimak). Increase in precipitation during monsoon season with peak in summer for Murghab and Shaimak in the most eastern part.
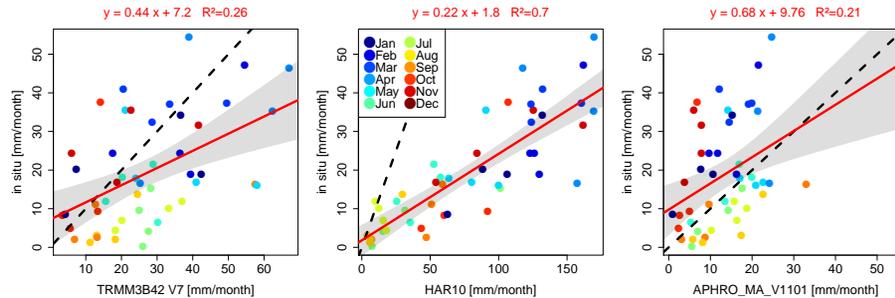
Figure A2. Comparison of precipitation datasets with in situ data on a monthly scale. Color code for months indicates systematic under- and overestimations for TRMM3B42 V7 and APHRO_MA_V1101. Grey-shaded area marks 95 % modelled confidence interval.